DOKUZ EYLUL UNIVERSITY

GRADUATE SCHOOL OF NATURAL AND APPLIED SCIENCES

NUMERICAL STUDY ON THE OPTIMIZATION OF PROCESS PARAMETERS IN FRICTION STIR WELDING

by

Mustafa TABANOĞLU

August, 2012

İZMİR

NUMERICAL STUDY ON THE OPTIMIZATION OF PROCESS PARAMETERS IN FRICTION STIR WELDING

A Thesis Submitted to the

Graduate School of Natural and Applied Sciences of Dokuz Eylül University
In Partial Fulfillment of the Requirements for the Degree of Master of Science
in Mechanical Engineering, Mechanic Program

by
Mustafa TABANOĞLU

August, 2012
İZMİR

M.Sc THESIS EXAMINATION RESULT FORM

We have read the thesis entitled "**NUMERICAL STUDY ON THE OPTIMIZATION OF PROCESS PARAMETERS IN FRICTION STIR WELDING**" completed by **MUSTAFA TABANOĞLU** under supervision of **ASSOC. PROF. BİNNUR GÖREN KIRAL** and we certify that in our opinion it is fully adequate, in scope and in quality, as a thesis for the degree of Master of Science.

Assoc. Prof. Binnur GÖREN KIRAL

Supervisor

(Jury Member)   (Jury Member)

Prof.Dr. Mustafa SABUNCU

Director

Graduate School of Natural and Applied Sciences

ACKNOWLEDGEMENTS

I would like to thank my supervisor, Assoc. Prof. Dr. Binnur GÖREN KIRAL for providing excellent guidance, continuous encouragement and her support during this study.

I would like to thank to Tirsan Kardan A.Ş. for usage of HyperWorks software.

I would also like to thank my colleagues Bengi ÖZBAĞCI, Levent Sacit AKBOY and my friend Görkem TOPÇUOĞLU for supporting.

I am greatly indebted to my family for their encouragement and moral support.

<div align="right">Mustafa TABANOĞLU</div>

NUMERICAL STUDY ON THE OPTIMIZATION OF PROCESS PARAMETERS IN FRICTION STIR WELDING

ABSTRACT

Friction stir welding is a new solid-state joining process. This welding method is used widely in automotive, aerospace, shipping, railway rolling stock and machine industry. This method can be used to join high-strength aluminum alloys and other metallic alloys that are hard to join by conventional welding processes.

The aim of this thesis is to model friction stir welding of 6061 and 7075 aluminum alloys using the finite element method. For this purpose, three-dimensional models were carried out by using HyperMesh and HyperXtrude commercial softwares. Temperature and stress distributions in the welded aluminum plate during the welding operation were obtained considering the mechanical properties changing with respect to the temperature. Effect of the transverse and rotational speeds of the pin on the temperature and stress distributions was examined.

The results obtained by the finite element analyses were presented in tabular form and graphically. It was concluded that temperature increases during the welding as transverse speed decreases and rotational speed increases. It was observed that the results indicate good agreement with the results in the literature.

Keywords: Friction stir welding, aluminum alloys, finite element method.

SÜRTÜNME KARIŞTIRMA KAYNAĞINDAKİ PROSES PARAMETRELERİNİN OPTİMİZASYONU ÜZERİNE SAYISAL ÇALIŞMA

ÖZ

Sürtünme karıştırma kaynağı yeni bir katı hal birleştirme işlemidir. Bu kaynak yöntemi otomotiv, havacılık, gemi taşımacılığı, raylı sistemler ve makine endüstrisinde yaygın olarak kullanılmaktadır. Bu yöntem klasik kaynak yöntemleri ile birleştirilmesi zor olan yüksek mukavemetli alüminyum alaşımları ve diğer metal alaşımların birleştirilmesinde kullanılabilmektedir.

Bu tezin amacı sonlu elemanlar yöntemi kullanarak AA6061 ve AA7075 alüminyum alaşımlarının sürtünme karıştırma kaynağını modellemektir. Bunun için HyperMesh ve HyperXtrude ticari programları kullanılarak üç boyutlu modeller oluşturulmuştur. Sıcaklığa göre değişen malzeme özellikleri göz önünde bulundurularak kaynak işlemi esnasında kaynaklanan alüminyum plakadaki sıcaklık ve gerilme dağılımları elde edilmiştir. Pim ilerleme ve dönüş hızlarının sıcaklık ve gerilme dağılımları üzerine etkisi incelenmiştir.

Sonlu elemanlar analizlerinden elde edilen sonuçlar tablo formunda ve grafik olarak sunulmuştur. İlerleme hızı azalıp dönüş hızı arttıkça kaynak esnasında sıcaklığın arttığı sonucuna varılmıştır. Sonuçların literatürdeki sonuçlarla uyum gösterdiği gözlemlenmiştir.

Anahtar sözcükler: Sürtünme karıştırma kaynağı, alüminyum alaşımlar, sonlu elemanlar yöntemi.

CONTENTS

CHAPTER ONE
INTRODUCTION

1.1. Introduction

Friction Stir Welding (FSW) was invented by Wayne Thomas at TWI Ltd in 1991 and overcomes many of the problems associated with traditional joining techniques. FSW is a solid state process which produces welds of high quality in difficult to weld materials such as aluminium and is fast becoming the process of choice for manufacturing light weight transport structures such as boats, trains and aeroplanes.(http://www.twi.co.uk/technologies/welding-coating-and-material-processing/friction-stir-welding/).

Friction stir welding (FSW) is a relatively new welding process that may have significant advantages compared to the fusion processes as follow: Joining of conventionally non-fusion weldable alloys, reduced distortion and improved mechanical properties of weldable alloys joints due to the pure solid-state joining of metals. Friction stir welding (FSW) is a relatively new, state-of the- art solid state joining process. This metal joining technique is derived from the conventional friction welding. In a typical FSW, a rotating cylindrical pin tool is forced to plunge into the plates to be welded (i.e. workpiece) and moved along their contact line. During this operation, frictional heat that is generated by contact friction between the tool and workpiece softens the material. The plasticized material is stirred by the tool and forced to "flow" to the side and the back of the tool as the tool advances. As the temperature cools down, a solid continuous joint between the two plates is then formed. Because the highest temperature in the FSW process is lowed than the melting temperature of the workpiece material, FSW yields fine microstructures, absence of cracking, low residual distortion and no loss of alloying elements that are the main advantages of this solid phase process. Nevertheless, as in the traditional fusion welds, a softened heat affected zone and a tensile residual stress parallel to the weld also exist (Zhu and Chao,2003).

It has become a unique technique well suited for joining many hard-to-weld metals, especially the high strength aluminum alloys and some dissimilar metals. Compared with the conventional welding processes, FSW possesses many advantages over traditional fusion joining techniques, such as no melting, low defect and low distortion, and FSW can even join thin and thick sections. This new technique is being successfully applied to the aerospace, automobile, and shipbuilding industries and opens up a broad avenue of joining technology development and research (Zhang, Zhang and Chen, 2005).

The heat transfer process is one of the most important aspects in the FSW study. A good understanding of the heat transfer process in the workpiece can be helpful in predicting the thermal cycles in the welding workpiece, and the hardness in the weld zone, subsequently, can be helpful in evaluating the weld quality. A known temperature distribution is also important for calculating the temperature-dependent viscosity when modeling material flow (Song and Kovacevic, 2002).

Although it is a new welding technology, the FSW has been extensively studied in both numerically and experimentally. Chen and Kovacevic (2003) studied on the finite element analysis of the thermal history and thermomechanical process in the butt-welding of aluminum alloy 6061- T6. The model used in this study incorporates the mechanical reaction of the tool and thermomechanical process of the welded material. The heat source incorporated in the model involves the friction between the material and the probe and the shoulder. In order to provide a quantitative framework for understanding the dynamics of the FSW thermomechanical process, the thermal history and the evolution of longitudinal, lateral, and through-thickness stress in the friction stirred weld are simulated numerically. The X-ray diffraction (XRD) technique is used to measure the residual stress of the welded plate, and the measured results are used to validate the efficiency of the proposed model. The relationship between the calculated residual stresses of the weld and the process parameters such as tool traverse speed is presented. It is anticipated that the model can be extended to optimize the FSW process in order to minimize the residual stress of the weld (Chen and Kovacevic, 2003)

Zhang and Zhang (2008) developed a thermo-mechanical model to predict the material deformations and temperature histories in the friction stir welding (FSW) process. Based on this model, the effects of the welding parameters on temperatures and material behaviors are investigated. Numerical results indicate that the maximum temperature in the FSW process can be increased with the increase of the rotating speed. The increase of the welding speed can lead to the obvious increase of the efficient input power for FSW system. The material particles on the top surface do not enter into the wake and just pile up at the border of the wake at the retreating side and this is the reason for the formation of the weld fash in FSW. Both the increase of the rotating speed and the decrease of thewelding speed can lead to the increase of the stirring effect of the welding tool, which can improve the friction stir weld quality. But when the rotating speed is increased, the weld fash becomes more obvious. When the welding speed becomes higher, the rotating speed must be increased simultaneously to avoid any possible welding defects such as void. The simultaneous increase of the rotating and the translating speeds of the welding tool can lead to the increase of the residual stress (Zhang and Zhang, 2008).

Zhang et al. (2005) developed solid mechanics-based finite element models and computational procedures to study the flowpatterns and the residual stresses in frictional stir welding (FSW). They presented two-dimensional results of the material flow patterns and the residual stresses and investigated the flow of metal during FSW is investigated using tracer particles. It was shown that the flows on the advancing side and retreating side are different. After several rotations the material which is rotating around the nib sloughs off in its wake of the pin, primarily on the advancing side. The residual stresses of the welded plate were investigated in this analysis. The distribution of the longitudinal residual stress along the direction perpendicular to the welding line is a double feature curve. They concluded that with the increase of the translational velocity, the maximum longitudinal residual stress can be increased (Zhang, Zhang, and Chen, 2005)

Thermo-mechanical simulation of friction stir welding can predict the transient temperature field, active stresses developed, forces in all the three dimensions and

may be extended to determine the residual stress. The thermal stresses constitute a major portion of the total stress developed during the process. Boundary conditions in the thermal modeling of process play a vital role in the final temperature profile. The heating and cooling rates with the peak temperature attained by the workpiece determine the thermal stress. Also, predicting realistic peak temperature becomes important as the operating temperature at the interface of tool-workpiece is very close to the solidus temperature of the aluminum workpiece. The convection heat-transfer coefficients of the surfaces exposed to air can be theoretically determined using Newton's law of cooling. Contact conductance depends on the pressure at the interface and has a non-uniform variation. The actual pressure distribution along the interface is dependent on the thermal stress from local temperature and non-linear stress–strain state. Therefore, applying an adaptive contact conductance can make the model more robust for process parameter variations. Soundararajan et al. (2005) developed a finite element thermo-mechanical model with mechanical tool loading considering a uniform value for contact conductance and used for predicting the stress at the workpiece and backplate interface. They used the pressure distribution contours for defining the non-uniform adaptive contact conductance used in the thermal model for predicting the thermal history in the workpiece. The thermo-mechanical model was then used in predict stress development in friction stir welding (Soundararajan, Zekovic, and Kovacevic, 2005).

Song and Kovacevic (2002) presented a three-dimensional heat transfer model for friction stir welding (FSW) and introduced a moving coordinate is introduced to reduce the difficulty of modeling the moving tool. Heat input from the tool shoulder and the tool pin were considered in the model. The finite difference method was applied in solving the control equations. A non-uniform grid mesh was generated for the calculation. FSW experiments have been done to validate the calculated results. They showed that the calculated results are good agreement with the experimental results. They concluded that preheat to the workpiece is beneficial to FSW. (Song and Kovacevic, 2002)

In this thesis, the finite element analyses have been performed to determine the temperature, stress and strain distribution in FSW of AA 6061 and AA 7075 alloys for different rotational and traverse speeds using hardened steel welding tool (H 13), by finite elements method using HyperMesh and HyperXtrude programs.

The dimension of aluminum plates and welding tools measures that were designed with Hypermesh, are identical with those that are used in real experiments. After the designing phase, illustrated welding metals and nozzles were transferred to HyperXtrude program and mesh modelling was done by finite elements method. Analysis was made by entering rotational and traverse speeds to the program.

In the second part of this study, advantages of friction stir welding, areas of the usage and mechanical properties of H 13 hardened steel welding tool, AA 6061 and AA 7075 aluminium alloys are presented.

In the third part of the study, AA 6061, AA 7075 aluminium alloys and H 13 hardened steel are designed by HyperXtrude software. The finite element model are generated.

In the fourth part, temperature and active stress distributions occurred during welding are determined using HyperXtrude software. Results obtained by the finite element analyses are compared and presented graphically and in tabular form.

CHAPTER TWO
FRICTION STIR WELDING

2.1 Friction Stir Welding (FSW)

Stir-welding, or friction stir-welding, is a technique which joins two pieces of sheet or thin plate by mechanical means. A schematic representation of the stir-welding process is shown in Fig. 1. The friction stir-welding tool (Fig. 2) consists of a shoulder, normal to the axis of rotation of the tool, and a smaller diameter pin connected to it. The tool shoulder, whose diameter is relatively large compared to that of the pin, acts as an upper backing bar to prevent material from being expelled from the workpiece. This minimizes the formation of voids in the weld zone. The pin is usually threaded in order to provide a large friction heating area, while maintaining the pin diameter relatively small (Ulysse 2002).
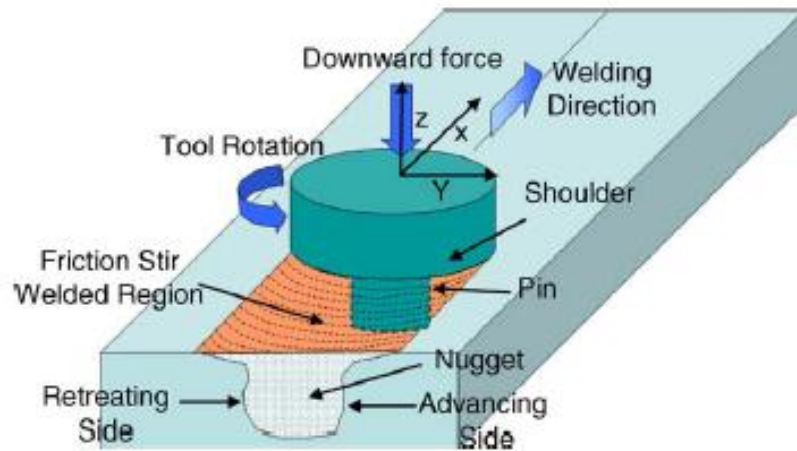
Figure 2.1 A schematic representation of the friction stir-welding process (Ulysse 2002, Mishra&Ma 2005).

2.1.1 Advantages of FSW

The process advantages result from the fact that the FSW process takes place in the solid phase below the melting point of the materials to be joined. The benefits include the ability to join materials that are difficult to fusion weld, for example, 2XXX and 7XXX aluminium alloys, magnesium and copper. Friction stir welding can use purpose-designed equipment or modified existing machine tool technology. The process is also suitable for automation and is adaptable for robot use. Other advantages are as follows:

- Low distortion and shrinkage, even in long welds
- Excellent mechanical properties in fatigue, tensile and bend tests
- No arc or fumes
- No porosity
- No spatter
- Can operate in all positions
- Energy efficient
- One tool can typically be used for up to 1000m of weld length in 6XXX series aluminium alloys
- No filler wire required
- No gas shielding for welding aluminium
- Some tolerance to imperfect weld preparations - thin oxide layers can be accepted
- No grinding, brushing or pickling required in mass production
- Can weld aluminium and copper of maximum 75mm thickness in one pass.

Despite being a relatively new technology, the benefits of friction stir welding mean that it is already in service with many companies worldwide for a wide range of applications. Safety critical items such as the fuel tanks on spacecraft, including the Space Shuttle, are now friction stir welded, as are many trains, cars and ships. Grades of aluminium that cannot be welded by traditional fusion - gas or electric arc - processes are readily welded by friction stir and the process is also being adopted

for welding magnesium and copper. (http://www.twi.co.uk/technologies/welding-coating-and-material-processing/friction-stir-welding/)

2.1.2 Applications

2.1.2.1 Shipbuilding and Marine Construction

The shipbuilding and marine industries are two of the first sectors that have adopted theprocess for commercial applications.

The process is suitable for the following applications:

- Panels for decks, sides, bulkheads and floors
- Hulls and superstructures
- Helicopter landing platforms
- Marine and transport structures
- Masts and booms, e.g. for sailing boats
- Refrigeration plant (http://www.twi.co.uk/technologies/welding-coating-and-material-processing/friction-stir-welding/)

2.1.2.2 Aerospace Industry

At present the aerospace industry is welding prototype and production parts by friction stir welding. Opportunities exist to weld skins to spars, ribs, and stringers for use in military and civilian aircraft. This offers significant advantages compared to riveting and machining from solid, such as reduced manufacturing costs and weight savings. Longitudinal butt welds in Al alloy fuel tanks for space vehicles have been friction stir welded and successfully used. The process could also be used to increase the size of commercially available sheets by welding them before forming.

The friction stir welding process can be considered for:
- Wings, fuselages, empennages

- Cryogenic fuel tanks for space vehicles

- Aviation fuel tanks

- External throw away tanks for military aircraft

- Military and scientific rockets

- Repair of faulty MIG welds (http://www.twi.co.uk/technologies/welding-coating-and-material-processing/friction-stir-welding/)

2.1.2.3 Railway Industry

The commercial production of high speed trains made from aluminium extrusions, which may be joined by friction stir welding, has been established.

Applications include:
- High speed trains

- Rolling stock of railways, underground carriages, trams

- Railway tankers and goods wagons

- Container bodies (http://www.twi.co.uk/technologies/welding-coating-and-material-processing/friction-stir-welding/)

2.1.2.4 Land Transportation

The friction stir welding process is currently being used commercially and is also being assessed by several automotive companies and suppliers.

Existing and potential applications include:
- Engine and chassis cradles

- Wheel rims

- Attachments to hydroformed tubes

- Space frames, e.g. welding extruded tubes to cast nodes

- Truck bodies & tail lifts for lorries

- Mobile cranes

- Armour plate vehicles

- Fuel tankers

- Caravans

- Buses and airfield transportation vehicles

    (http://www.twi.co.uk/technologies/welding-coating-and-material-
    processing/friction-stir-welding/)

CHAPTER THREE

MODELLING AND ANALYSIS OF FRICTION STIR WELDING

In this study, three-dimesional finite element analyses were performed in order to obtain the temperature, stress and strain distribution in the aluminum alloy plates during the friction stir welding. HyperMesh and HyperXtrude softwares were used to model and analyse FSW, respectively.

3.1 Mechanical and Physical Properties of Workpiece and Tool Materials

AA 6061 and AA 7075 aluminium alloys were used as the work-piece, and the tool material was chosen as H13 hardened steel. Tables 3.1-3.2 show the mechanical properties of AA 6061, AA7075 and H13 at room temperature, respectively.

Table 3.1 Mechanical properties of AA 6061 and AA 7075.

Mechanical properties	AA 6061	AA 7075
Density (kg/m^3)	2700	2810
Specific Heat (J/kgK)	896	960
Conductivity (W/mK)	180	173
Coeff Of Thermal Expansion (1/K)	$1 \cdot 10^{-5}$	$1 \cdot 10^{-5}$
Volumetric Heat Source (W/m^3)	0	0
Reference Temperature (K)	293	293
Liquidus Temperature (K)	925	908
Solidus Temperature (K)	855	750
Young Modulus (GPa)	60	70
Poisson Ratio	0.35	0.35

Table 3.2 The mechanical properties of H13

Density (kg/m^3)	7870
Specific Heat (J/kg-K)	460
X Conductivity (W/mK)	24.3
Y Conductivity (W/mK)	24.3
Z Conductivity (W/mK)	24.3
Volumetric Heat Source (W/m^3)	0
Young Modulus (GPa)	210
Poisson Ratio	0.35

Tables 3.3-3.5 show the temperature dependent mechanical properties of AA6061 and AA 7075 (Cayless, 1992).

Table 3.3 Mechanical properties of AA6061 with respect to temperature.

Temperature (^{o}C)	Yield Strength (MPa)	Tensile Strength (MPa)
24	276	310
100	262	290
149	214	234
204	103	131
260	34	51
316	19	32
371	12	24

Table 3.4 Mechanical properties of AA7075 with respect to temperature.

Temperature (^{o}C)	Yield Strength (MPa)	Tensile Strength (MPa)
24	503	572
100	448	483
149	186	214
204	87	110
260	62	76
316	45	55
371	32	41

Table 3.5 Brinell hardness

	AA 6061	**AA 7075**
Brinell Hardness (500 kg, 10 mm, 30 s)	95	150

Figures 3.1-3.4 show variation of viscosity and strain rate according to the temperature for AA 6061 and AA 7075 aluminium alloys.
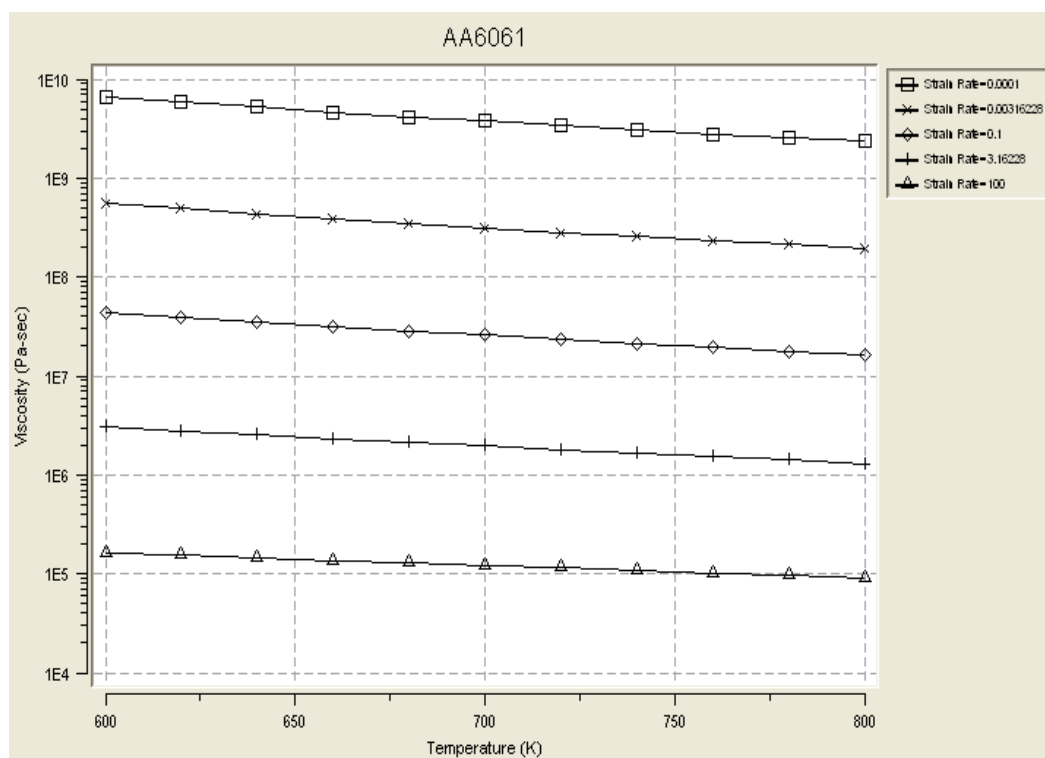
Figure 3.1 Viscosity - temperature graphic of AA 6061
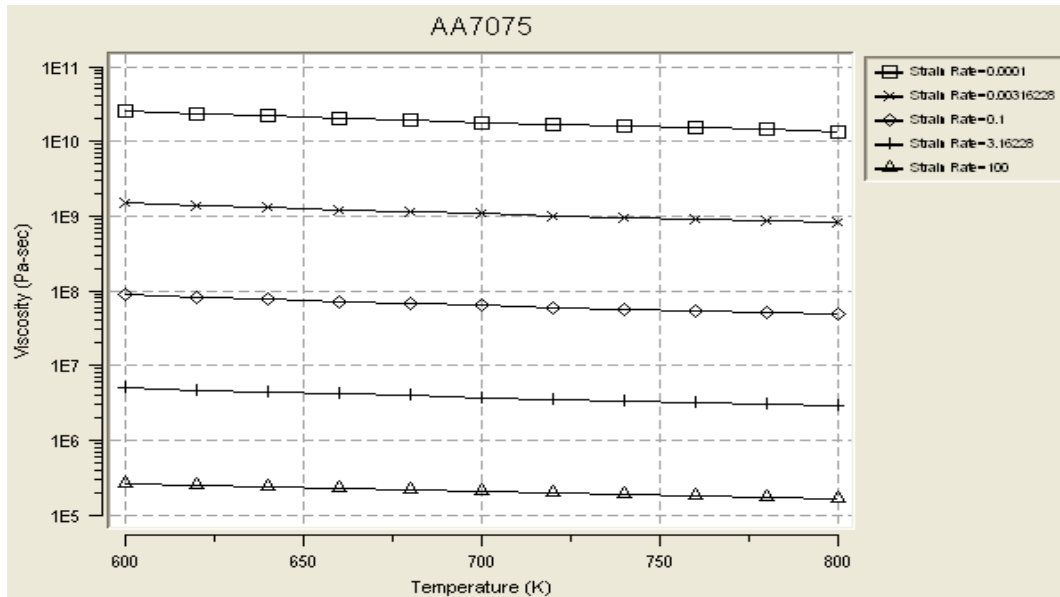
Figure 3.2 Viscosity - temperature graphic of AA 7075
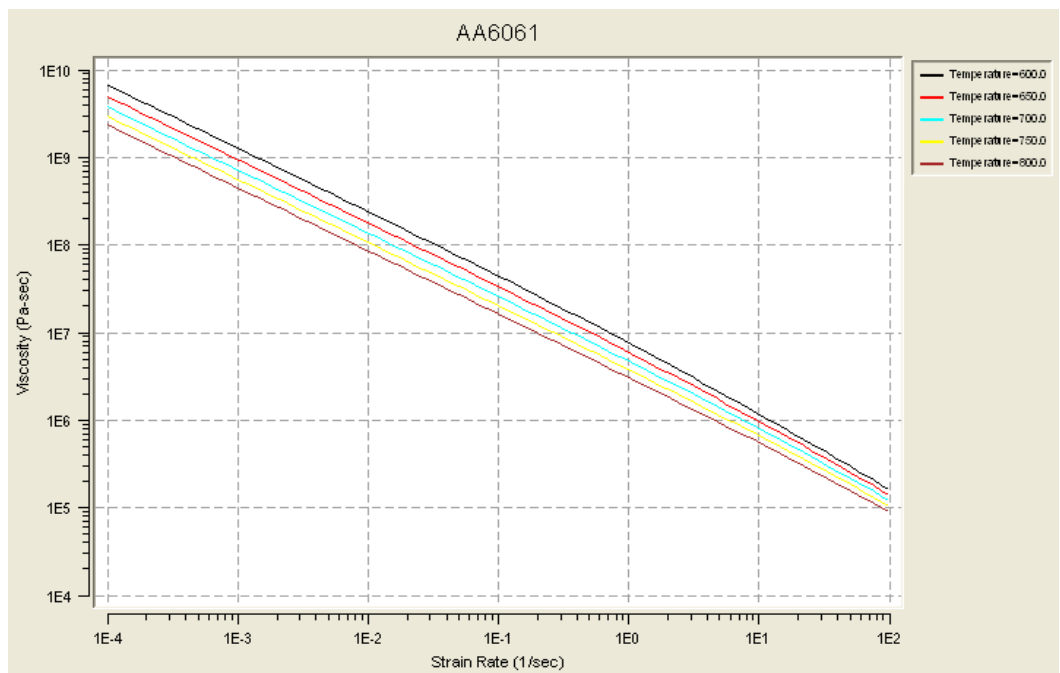
Figure 3.3 Viscosity - strain rate graphic of AA 6061
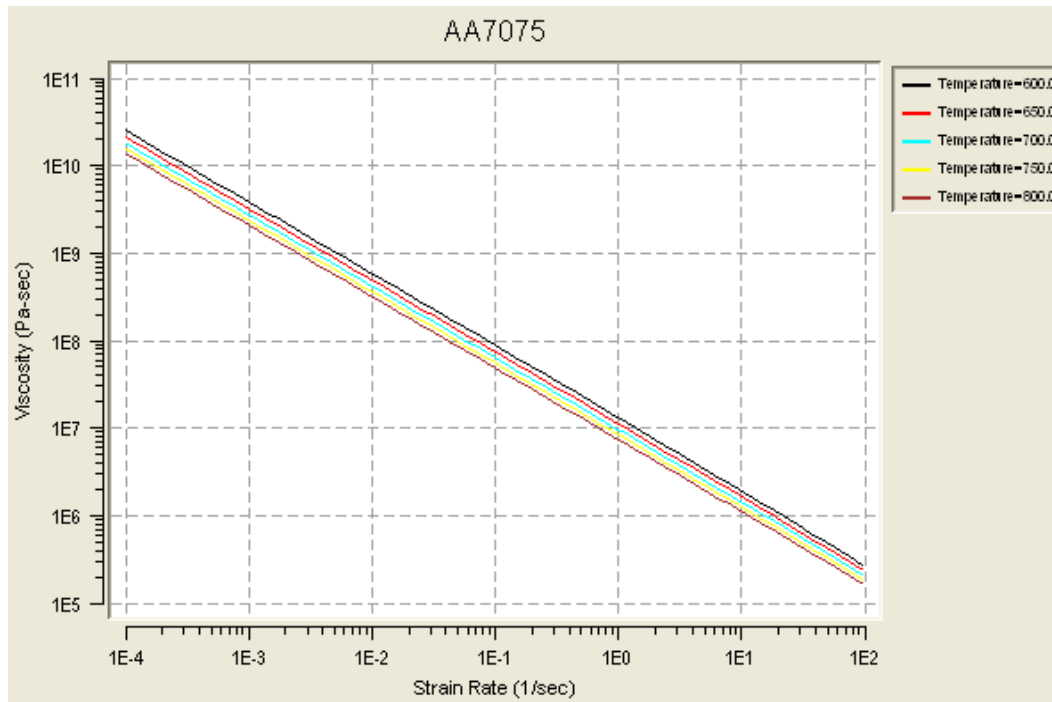
Figure 3.4 Viscosity - strain rate graphic of AA 7075

3.2 Modeling of Workpiece and Tool

Figure 3.5 shows the shape of workpieces used in this study. Dimension of the plate can be seen in Figure 3.6. In Fig 3.6 the measurements of work-piece and tool are shown. Work piece 1 and workpiece 2 are of the same materials. Both the work-pieces' measurements are identical to each other. The length, width and depth of workpiece are 300 mm, 200 mm and 3.1 mm, respectively.
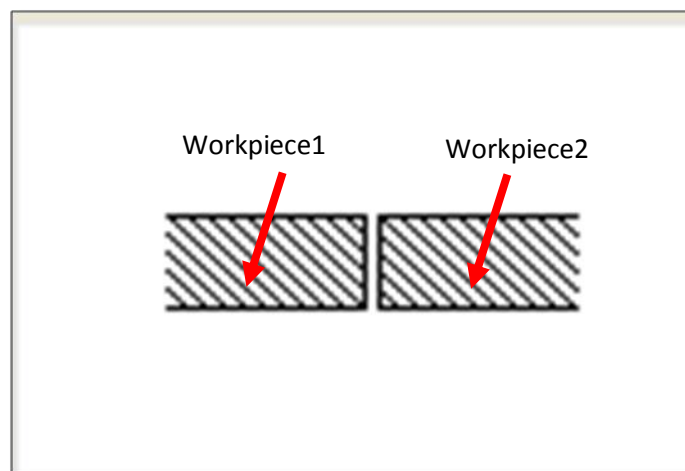
Figure 3.5 Aluminum alloy plates
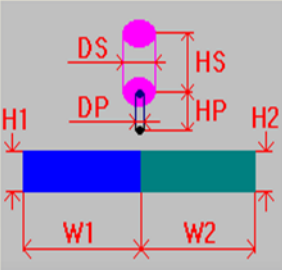
Figure 3.6 Dimensions of workpieces and tool

Total height and radius of the tool were chosen as 150 mm and 16 mm, respectively. The radius and height of the device on tool tip were assumed as 4 mm and 2.79 mm, respectively. The angle between tool and the workpiece is 0°.
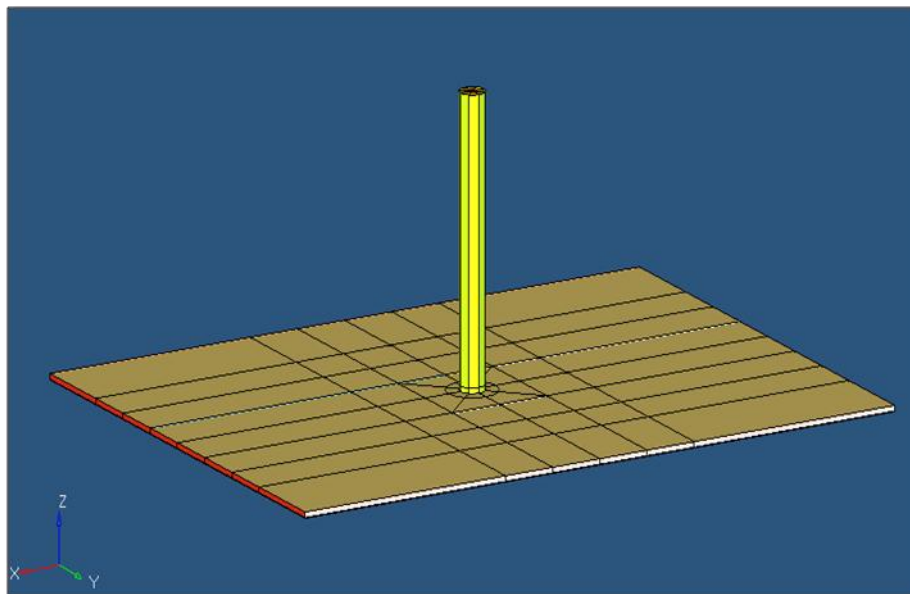
Figure 3.7 Solid model of workpieces and tool

3.3 Meshing

Finite element method is a reliable computational technique to analyse and illustrate engineering designs. Finite element method uses the information from all of the model's subelements to appoint the behaviour of the model.

In this part, the objective is to produce finite element mesh (Fig 3.8) of all the workpieces that will be used in FSW analysis and give brief information on this mesh. In this study, finite element method is used in order to be able to compare all the analysis results.
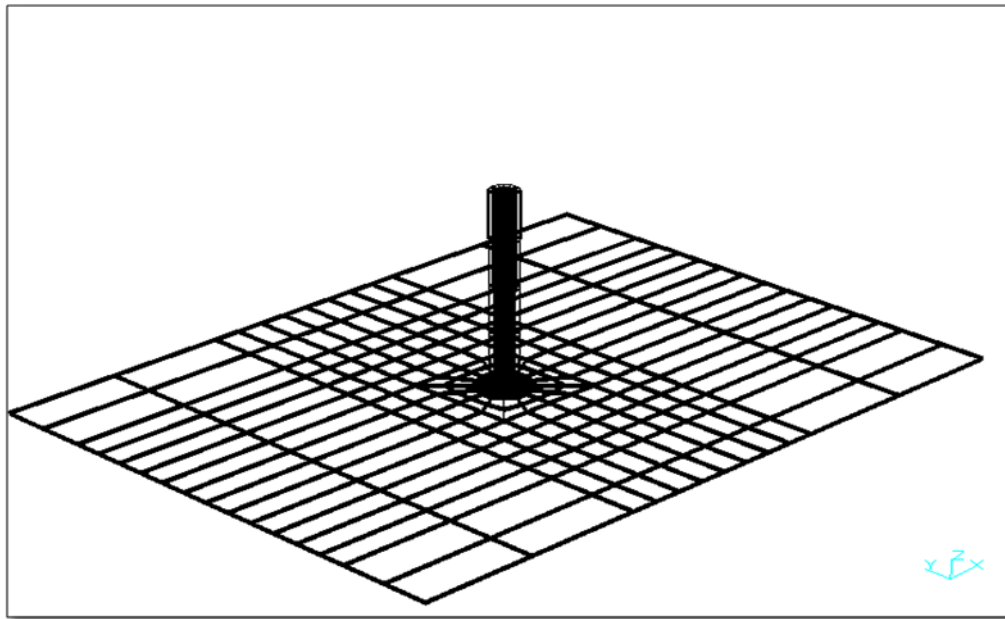
Figure 3.8 Finite element modeling of FSW

After the workpieces are modeled and meshed using HyperWorks, the model is transferred to HyperXtrude software and two workpieces of AA 6061 and AA 7075 aluminium alloys for various conditions of FSW to simulate the welding process.

CHAPTER FOUR
RESULTS

Finite element analyses were performed both AA6061 and AA7075. Pin rotational speeds were chosen as 800, 1000 and 1200 revolution per minute. The finite element analyses were repeated for transverse speeds of 2.5 and 5 mm/s for all rotational speeds. Temperature and stress distribution obtained by the finite element analyses were presented as tabular and graphically.

4.1 AA 6061

4.1.1 Pin rotational speed ω = 800 rpm and pin transverse speed v = 2.5 mm/s

Table 4.1 Friction Welding Parameters of AA 6061 for ω= 800 rpm v=2.5 mm/s

Pin Diameter (mm)	4
Pin Height (mm)	2.79
Tilt Angle (deg)	0
Pin Rotational Speed (rpm)	800
Pin Translational Speed (rpm)	2.5
Shoulder Diameter (mm)	16
Shoulder Height (mm)	150
Reference Temperature (K)	293

The dimensions of the workpieces are shown in Table 4.1. Pin rotational speed and traverse speed are ω = 800 rpm and v= 2.5 mm/s, respectively. The reference temperature is 20° C.

Fig 4.1 shows the temperature distribution of the workpieces joined by FSW during welding.
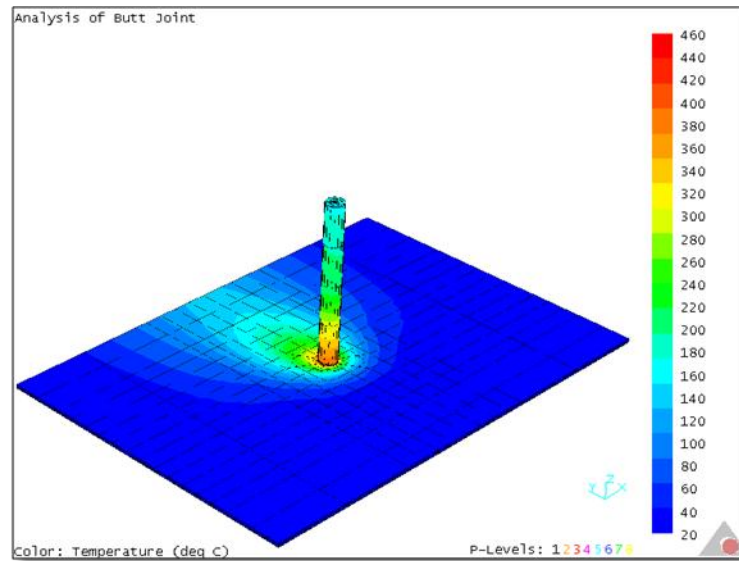
Figure 4.1 Temperature distribution of AA 6061 for ω=800 rpm and
v= 2.5 mm/s.

As shown in the figure, the maximum temperature reaches about 460 $^{\circ}$C on the tool. The maximum temperature of the plate is about 420 $^{\circ}$C.

Fig 4.2 - 4.7 present the stress distributions (σ_x, σ_y, σ_z, τ_{xy}, τ_{xz} and τ_{yz}) during the welding process.

Figure 4.2 σ_x stress distribution in the AA 6061 alloy plates during
welding for ω=800 rpm and v= 2.5 mm/s.

Figure 4.3 σ_y stress distribution in the AA 6061 alloy plates during welding for ω=800 rpm and v= 2.5 mm/s.
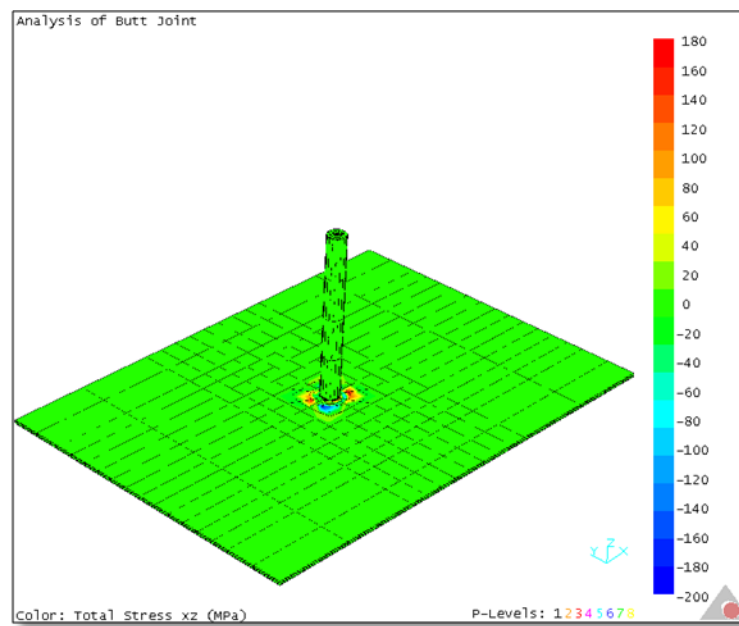

Figure 4.4 σ_z stress distribution in the AA 6061 alloy plates during welding for ω=800 rpm and v= 2.5 mm/s.
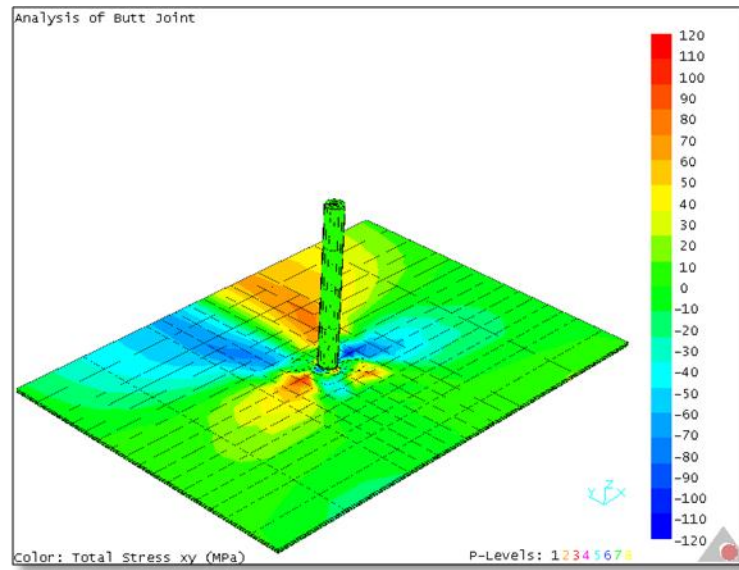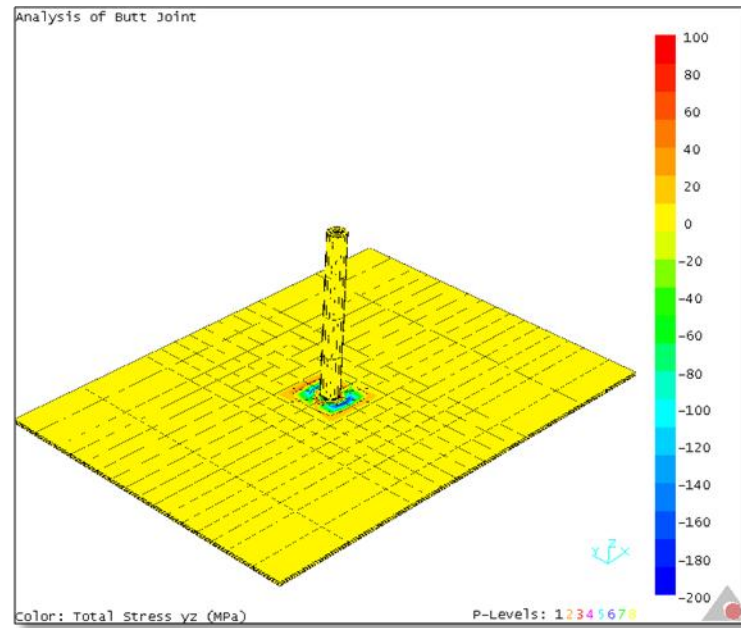
Figure 4.5 τ_{xy} stress distribution in the AA 6061 alloy plates during welding for ω=800 rpm and v= 2.5 mm/s.

Figure 4.6 τ_{xz} stress distribution in the AA 6061 alloy plates during welding for ω=800 rpm and v= 2.5 mm/s.

Figure 4.7 τ_{yz} stress distribution in the AA 6061 alloy plates during welding for ω=800 rpm and v= 2.5 mm/s.

Fig 4.8 shows the temperature variation during FSW on x, y, z coordinate plane coordinates (0;0;0), (0;10;0), (0;20;0), (0;30;0), (0;40;0) [mm].
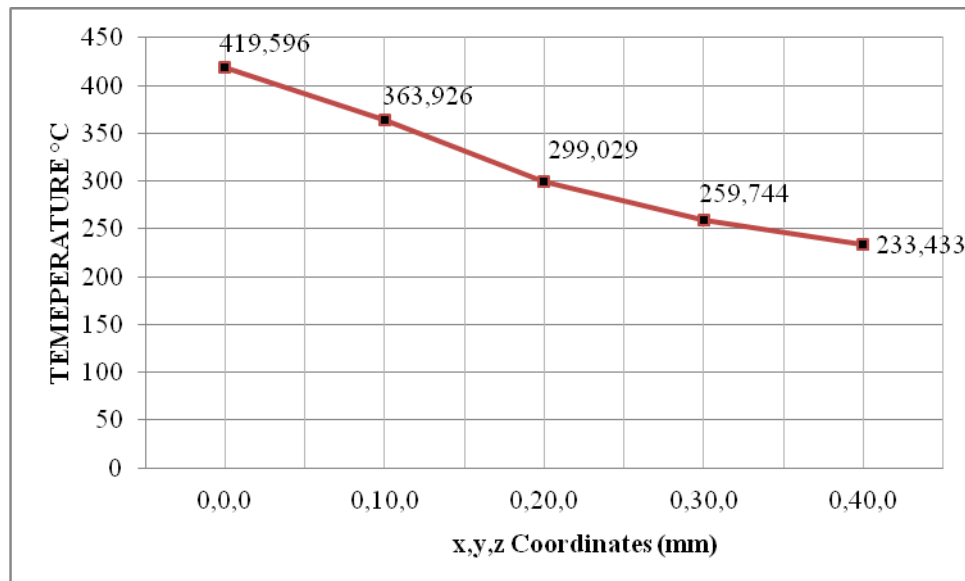
Figure 4.8 Temperatures at different coordinates for ω=800 rpm and v= 2.5 mm/s.

4.1.2 Pin rotational speed ω = 800 rpm and pin transverse speed v = 5 mm/s

Analyses were repeated for ω = 800 rpm and v = 5 mm/s to determine the effect of the transverse speed on the temperature and stress distribution.

Table 4.2 Friction welding parameters of AA 6061 for ω= 800 rpm and v= 5 mm/s

Pin Diameter (mm)	4
Pin Height (mm)	2.79
Tilt Angle (deg)	0
Pin Rotational Speed (rpm)	800
Pin Translational Speed (rpm)	5
Shoulder Diameter (mm)	16
Shoulder Height (mm)	150
Reference Temperature (K)	293

The dimensions of the workpieces and tool are shown in Table. 4.2. Rotational speed is ω= 800 rpm and traverse speed is v= 5 mm/s. The reference temperature is 20° C.

Figure 4.9 shows the distribution of temperature during the welding. The maximum temperature reaches about 440 ^{o}C on the tool. The maximum temperature of the plate is about 410 ^{o}C. As seen from Figures 4.1 and 4.9, temperature decreases as the transverse speed incerases.
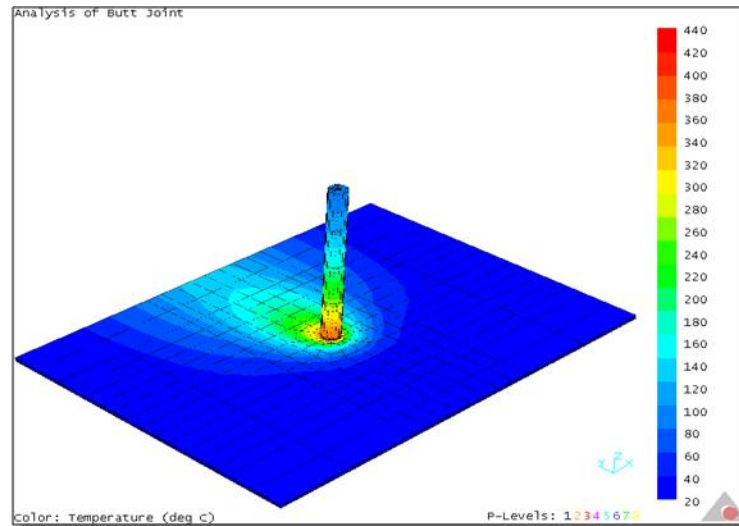
Figure 4.9 Temperature distribution of AA 6061 for ω=800 rpm and v=5 mm/s.

Figures 4.10 - 4.15 present the stress distributions (σ_x, σ_y, σ_z, τ_{xy}, τ_{xz} and τ_{yz}) during the welding process.
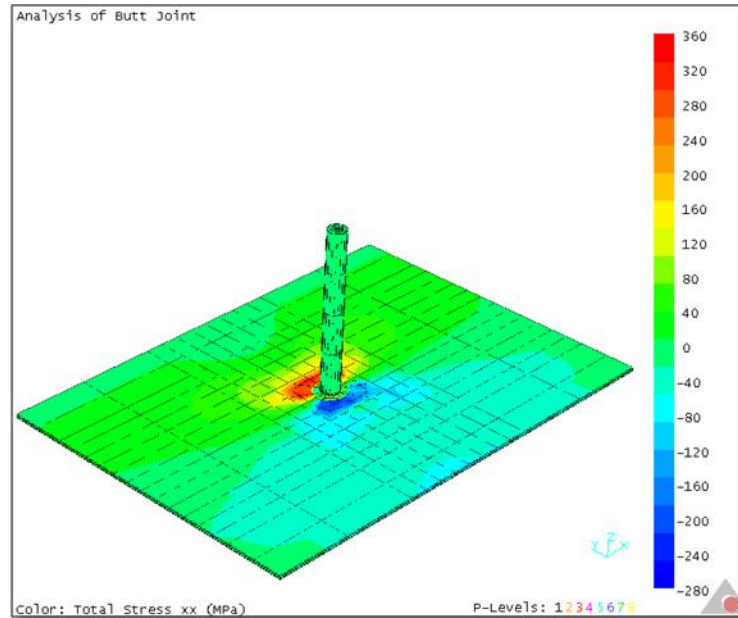

Figure 4.10 σ_x stress distribution in the AA 6061 alloy plates during

welding for ω=800 rpm and v= 5 mm/s.
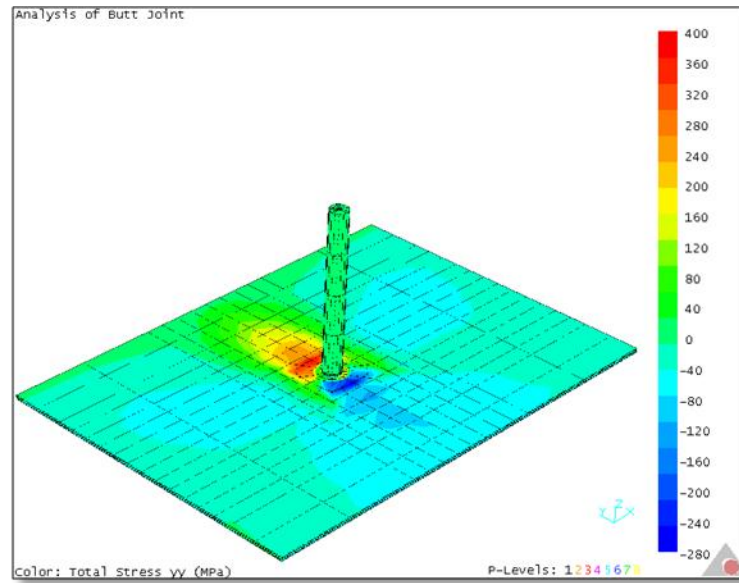
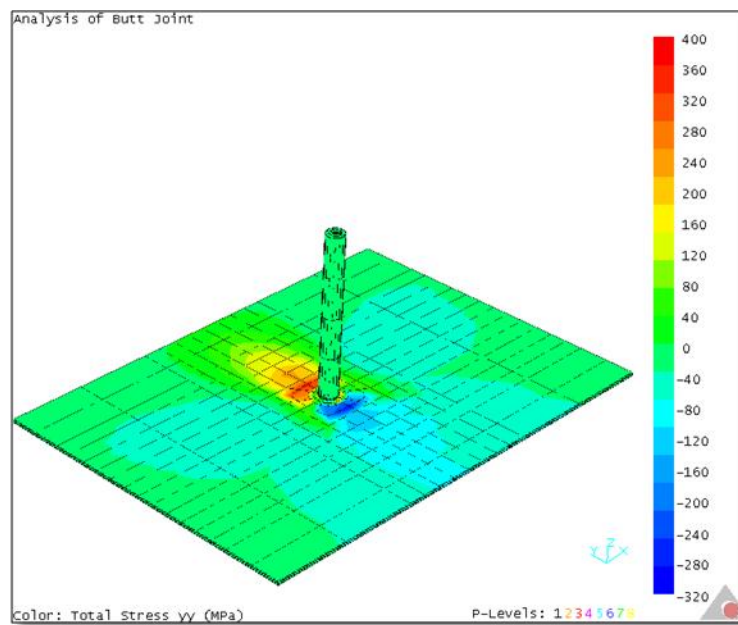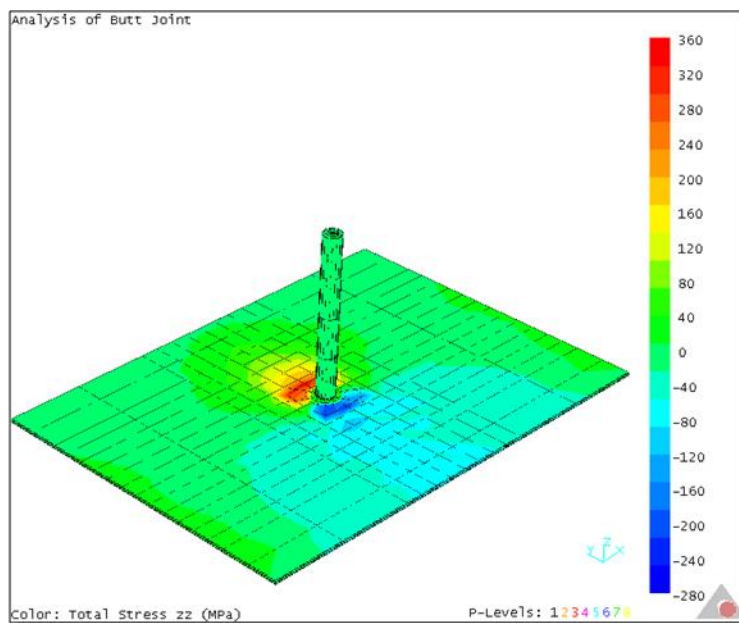Figure 4.11 σ_y stress distribution in the AA 6061 alloy plates during welding for ω=800 rpm and v= 5 mm/s.
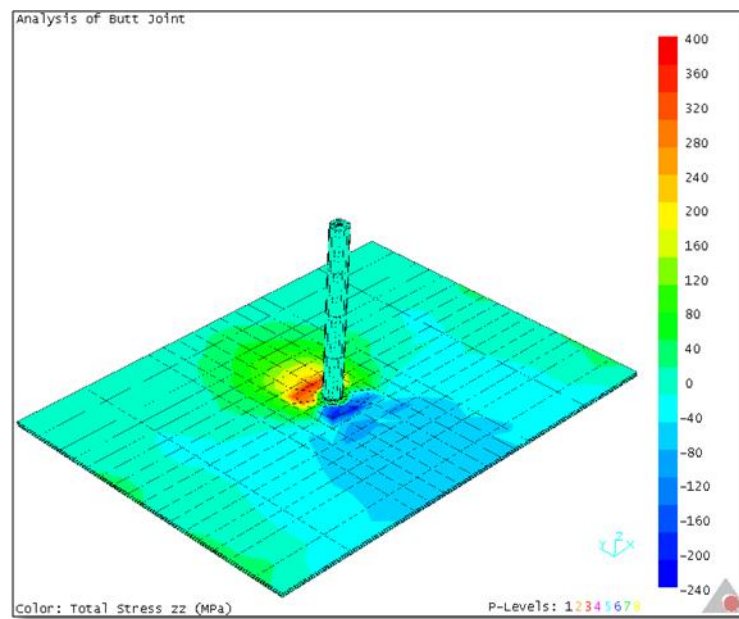
Figure 4.12 σ_z stress distribution in the AA 6061 alloy plates during welding for ω=800 rpm and v= 5 mm/s.
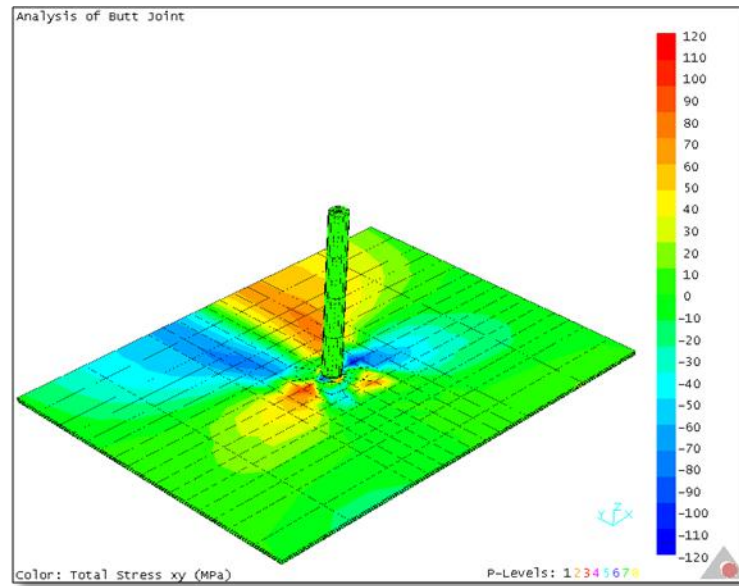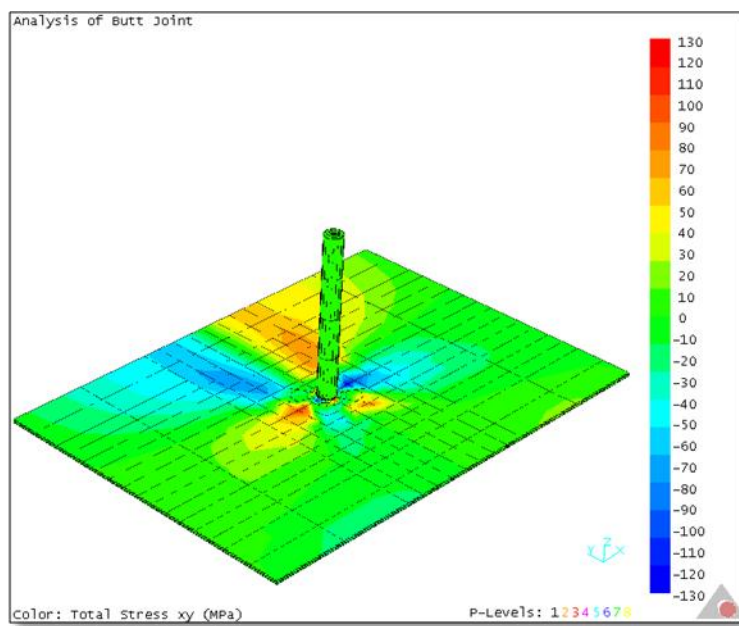
Figure 4.13 τ_{xy} stress distribution in the AA 6061 alloy plates during welding for ω=800 rpm and v= 5 mm/s.
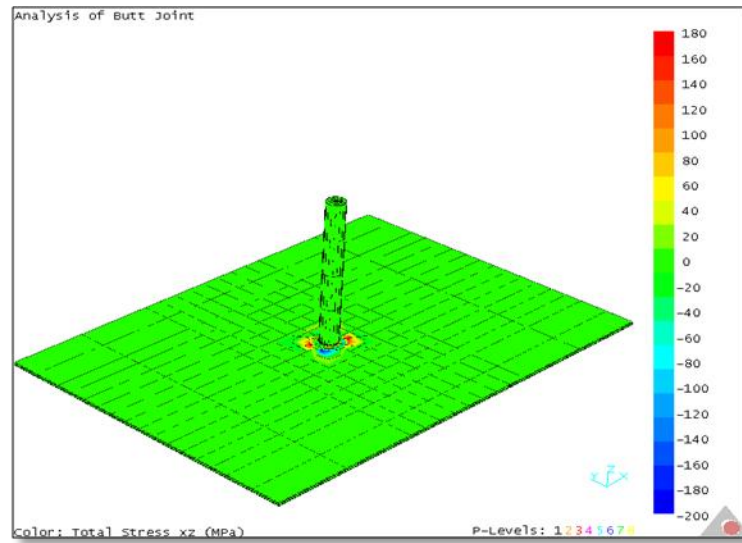

Figure 4.14 τ_{xz} stress distribution in the AA 6061 alloy plates during welding for ω=800 rpm and v= 5 mm/s.
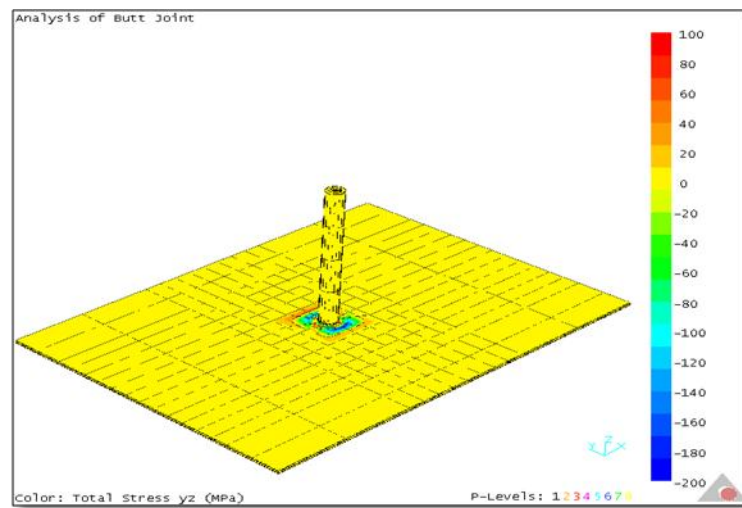
Figure 4.15 τ_{yz} stress distribution in the AA 6061 alloy plates during

welding for ω=800 rpm and v= 5 mm/s.

Figure 4.16 shows the temperature variation during FSW on x, y, z coordinate plane coordinates (0;0;0), (0;10;0), (0;20;0), (0;30;0), (0;40;0) [mm].
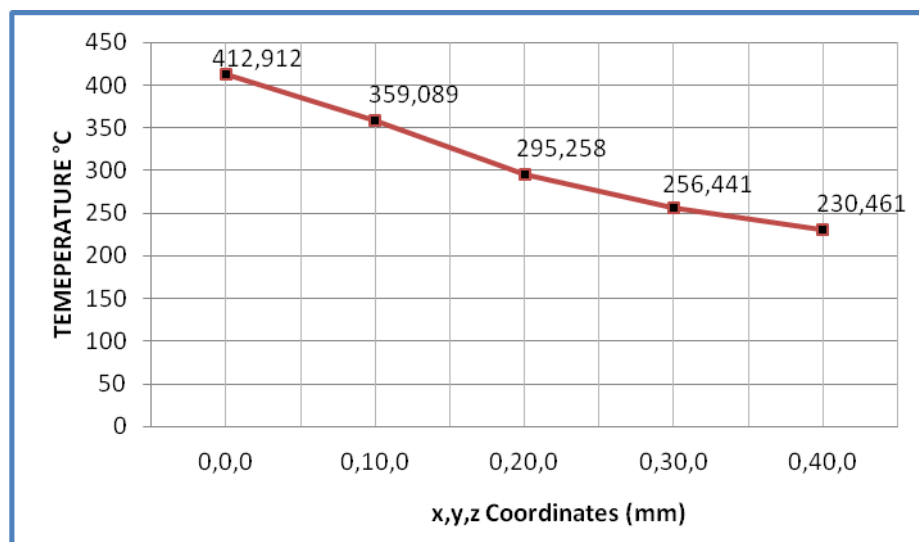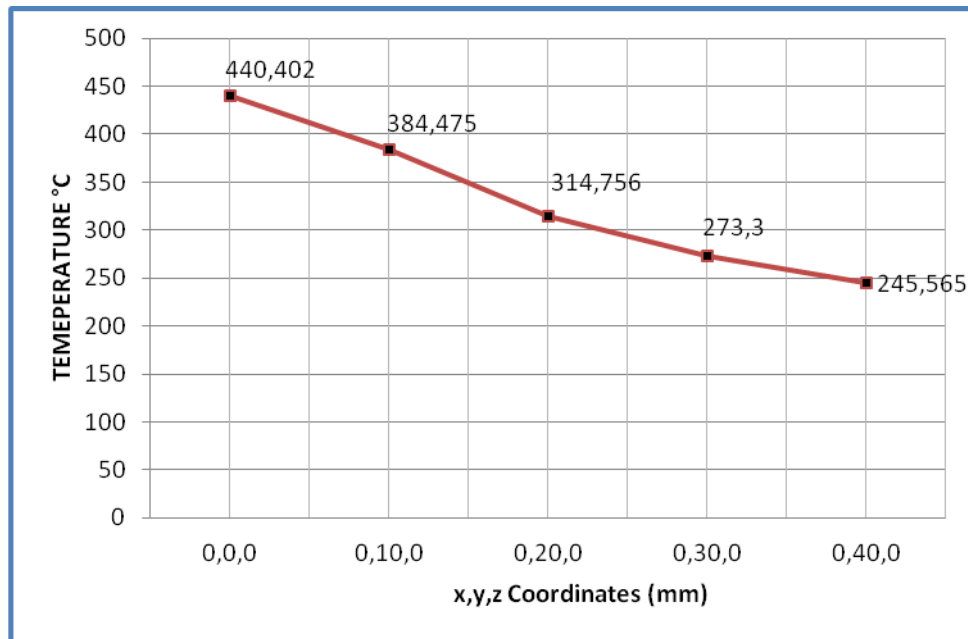

Figure 4.16 Temperatures at different coordinates for AA 6061 ω=800 rpm and v= 5 mm/s.

4.1.3 Pin rotational speed ω = 1000 rpm and pin transvers speed v = 2.5 mm/s

In order to determine the effect of the pin rotational speed, the finite element analyses were repeated for the rotational speeds of 1000 rpm. Table 4.3 presents this weld conditions.

Table 4.3 Friction welding parameters of AA 6061 for ω = 1000 rpm and v=2.5 mm/s

Pin Diameter (mm)	4
Pin Height (mm)	2.79
Tilt Angle (deg)	0
Pin Rotational Speed (rpm)	1000
Pin Translational Speed (rpm)	2.5
Shoulder Diameter (mm)	16
Shoulder Height (mm)	150
Reference Temperature (K)	293

Figure 4.17 shows the temperature distribution during the welding. As seen form the figure, temperature increases as the rotational speed increases compared to the results obtained by the analyses for 800 rpm. The maximum temperatures are 480 and 440 ^{o}C on the tool and plate, respectively.
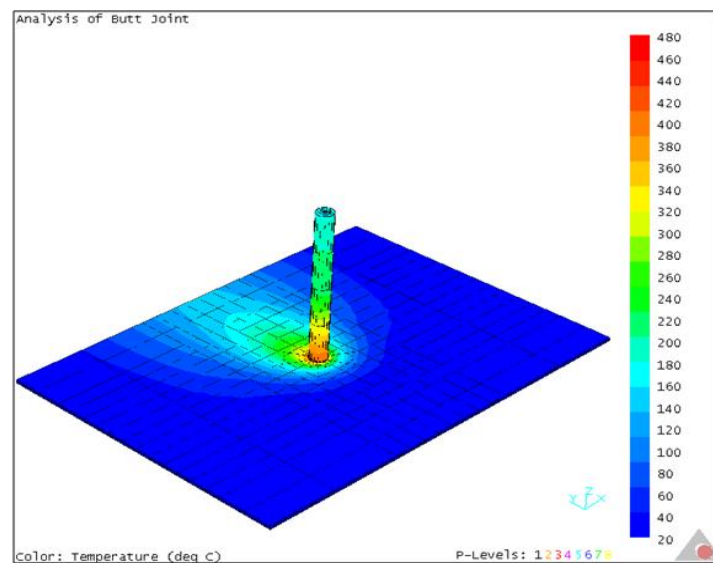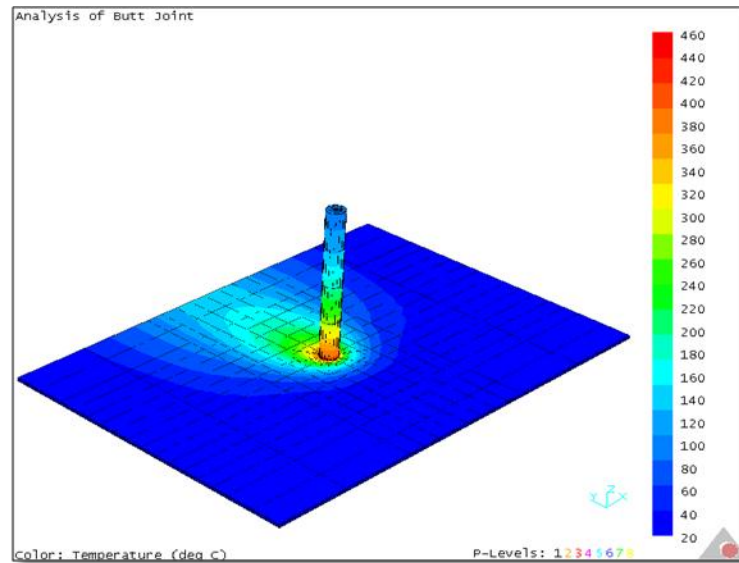

Figure 4.17 Temperature distribution of AA 6061 for ω= 1000 rpm
and v= 2.5 mm/s

Figures 4.18-4.23 show the stress distributions during the welding process for 1000 rpm.
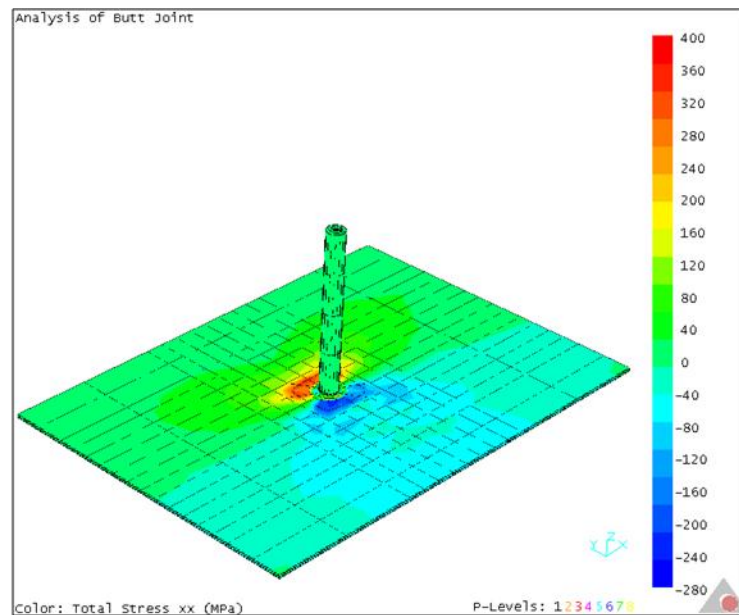

Figure 4.18 σ_x stress distribution in the AA 6061 alloy plates during welding for ω=1000 rpm and v=2.5 mm/s.
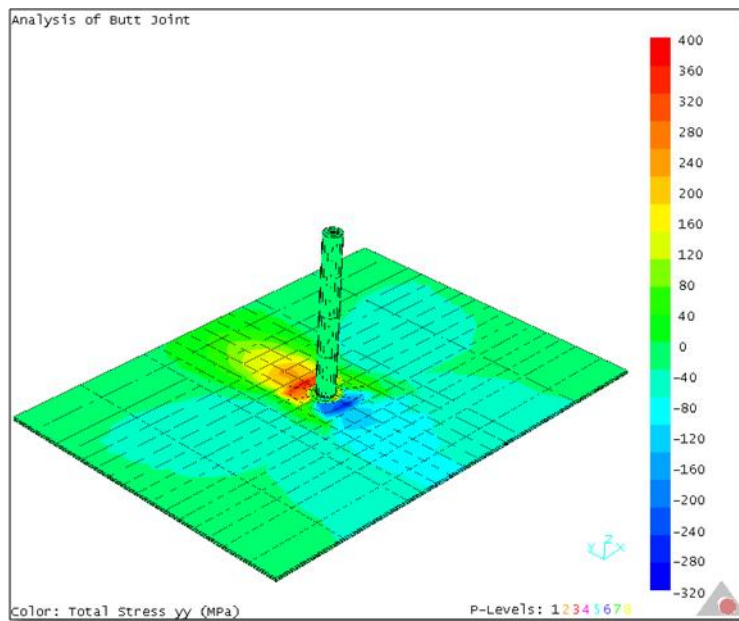

Figure 4.19 σ_y stress distribution in the AA 6061 alloy plates during welding for ω=1000 rpm and v=2.5 mm/s.
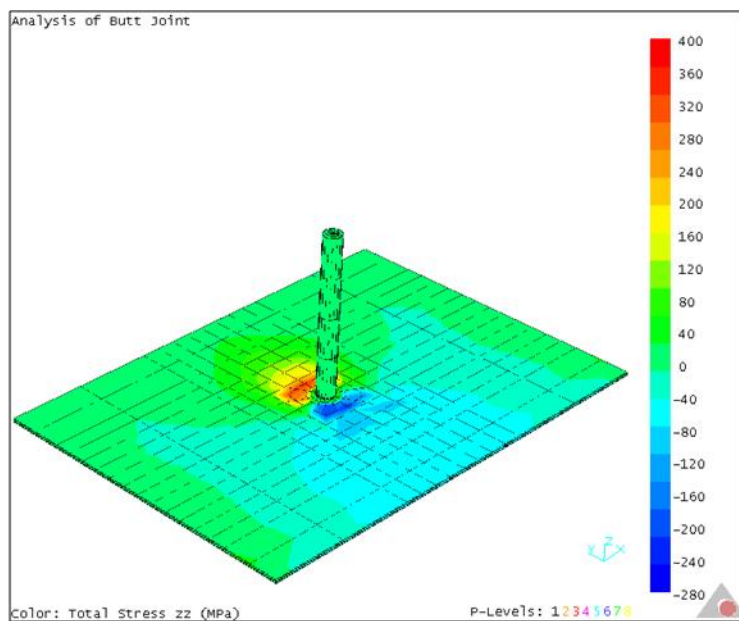
Figure 4.20 σ_z stress distribution in the AA 6061 alloy plates during welding for ω=1000 rpm and v=2.5 mm/s.

Figure 4.21 τ_{xy} stress distribution in the AA 6061 alloy plates during welding for ω=1000 rpm and v=2.5 mm/s.

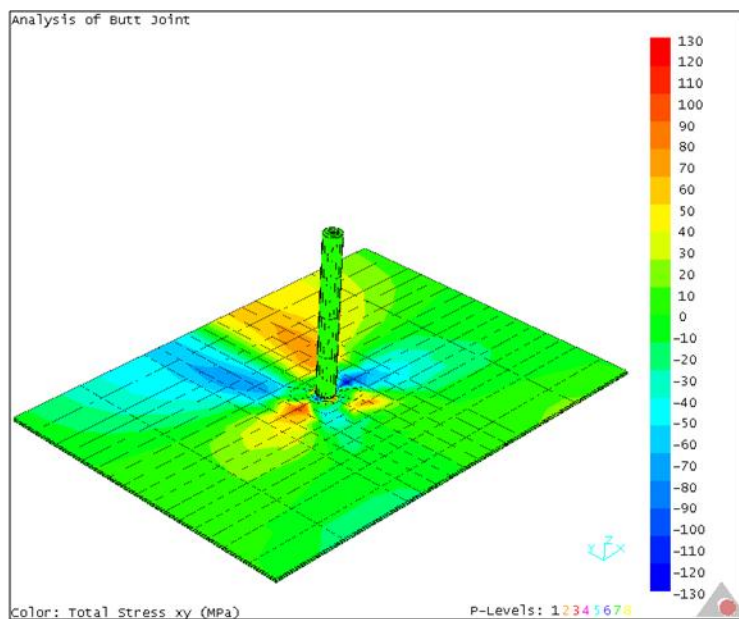Figure 4.22 τ_{xz} stress distribution in the AA 6061 alloy plates during welding for ω=1000 rpm and v=2.5 mm/s.

Figure 4.23 τ_{yz} stress distribution in the AA 6061 alloy plates during welding for ω=1000 rpm and v=2.5 mm/s.
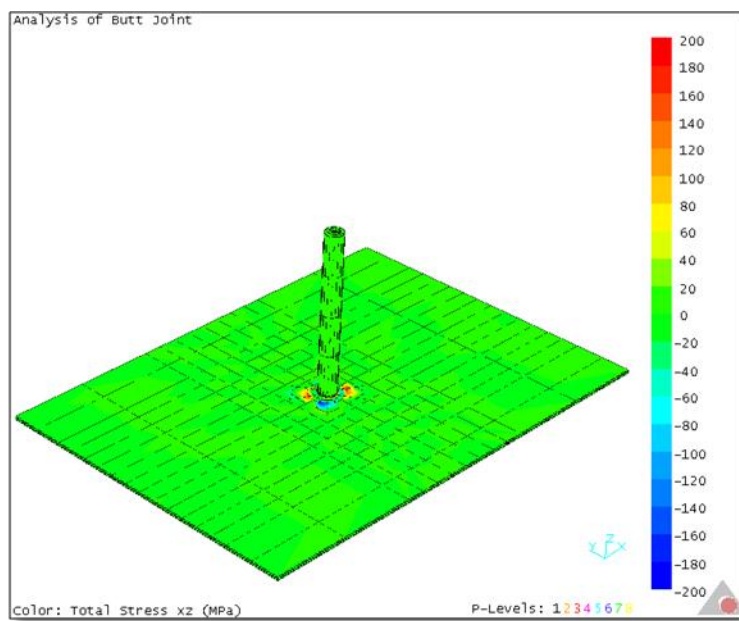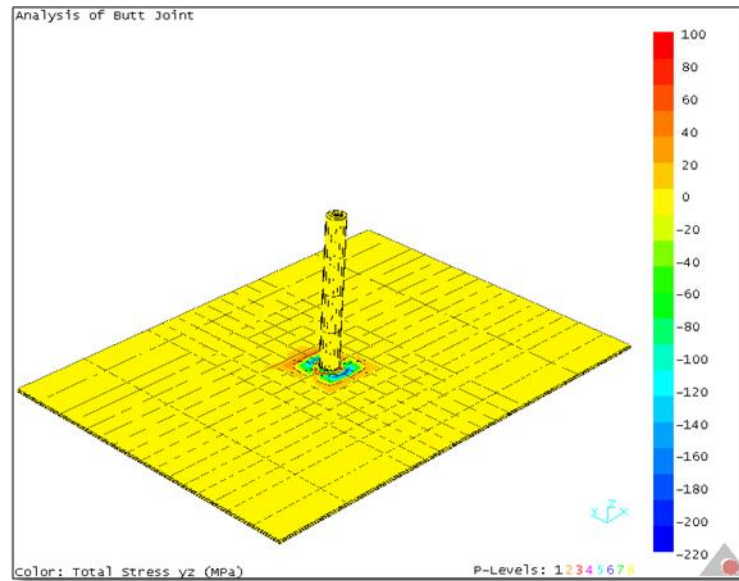
Figure 4.24 show the temperature variation during FSW on x, y, z coordinate plane coordinates (0;0;0), (0;10;0), (0;20;0), (0;30;0), (0;40;0) [mm].
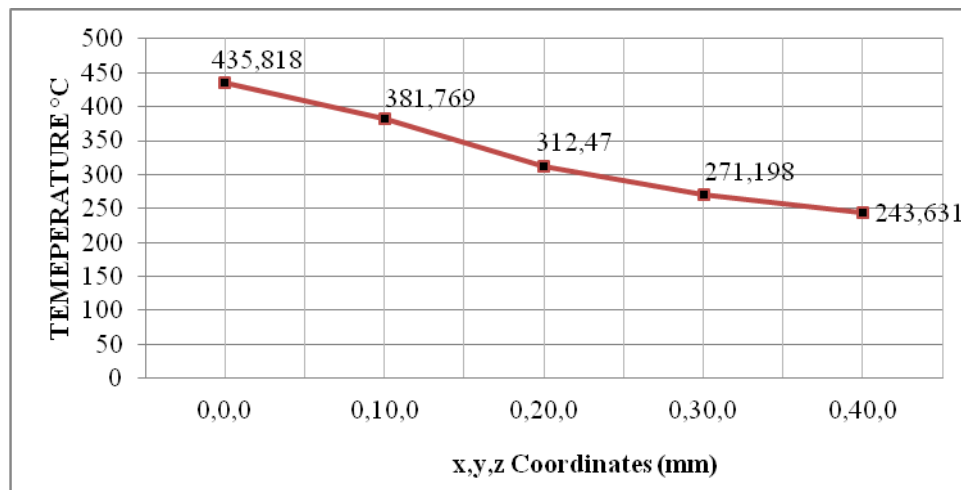
Figure 4.24 Temperatures at different coordinates for ω= 1000 rpm and v = 2.5 mm/s

4.1.4 Pin rotational speed ω = 1000 rpm and pin rotational speed v = 5 mm/s

In this section, the finite element analyses were performed for pin rotational speed of 1000 rpm and transverse speed of 5 mm/s. The welding conditions can be seen in Table 4.4.

Table 4.4 Friction welding parameters of AA 6061 for ω= 1000 rpm and v=5 mm/s

Pin Diameter (mm)	4
Pin Height (mm)	2.79
Tilt Angle (deg)	0
Pin Rotational Speed (rpm)	1000
Pin Translational Speed (rpm)	5
Shoulder Diameter (mm)	16
Shoulder Height (mm)	150
Reference Temperature (K)	293

Figure 4.25 shows the temperature distribution during the welding. The maximum temperatures are about 460 and 435 oC on the tool and plate, respectively. As seen from the figure the temperature decreases since the transverse speed increases.

Figure 4.25 Temperature distribution of AA 6061 for ω= 1000 rpm
and v = 5 mm/s

Figures 4.26 - 4.31 present the stress distributions (σ_x, σ_y, σ_z, τ_{xy}, τ_{xz} and τ_{yz}) during the welding process.

Figure 4.26 σ_x stress distribution in the AA 6061 alloy plates during
welding for ω=1000 rpm and v=5 mm/s.

Figure 4.27 σ_y stress distribution in the AA 6061 alloy plates during welding for ω=1000 rpm and v=5 mm/s.

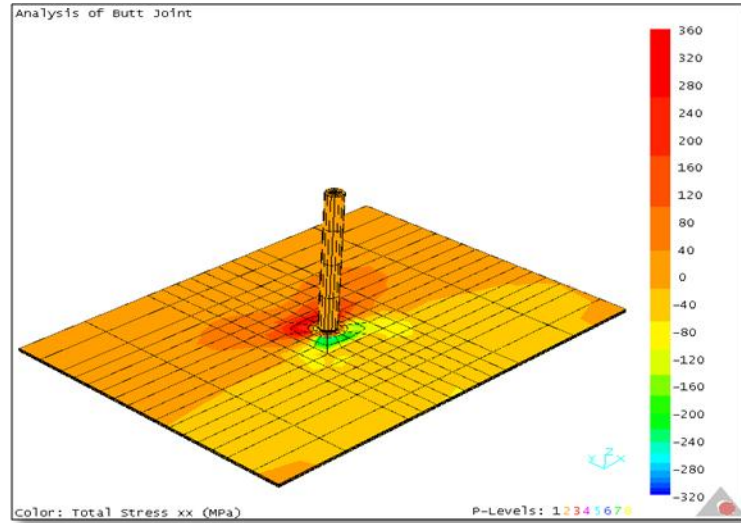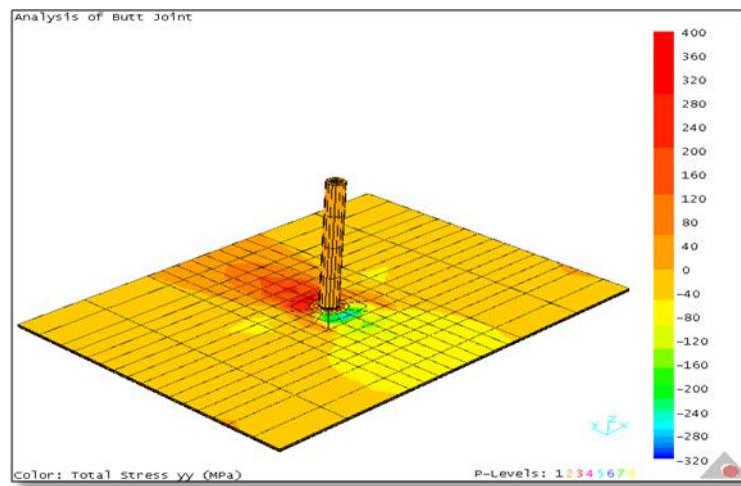Figure 4.28 σ_z stress distribution in the AA 6061 alloy plates during welding for ω=1000 rpm and v=5 mm/s.

Figure 4.29 τ_{xy} stress distribution in the AA 6061 alloy plates during welding for ω=1000 rpm and v=5 mm/s.

Figure 4.30 τ_{xz} stress distribution in the AA 6061 alloy plates during welding for ω=1000 rpm and v=5 mm/s.

Figure 4.31 τ_{yz} stress distribution in the AA 6061 alloy plates during
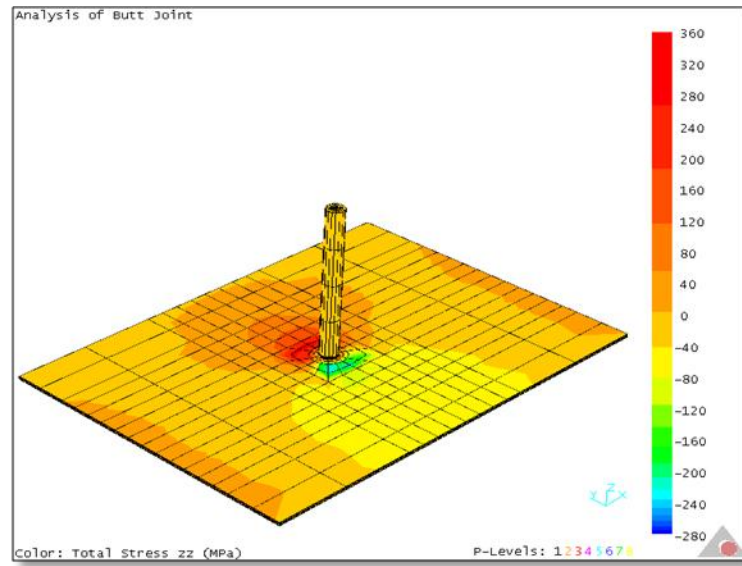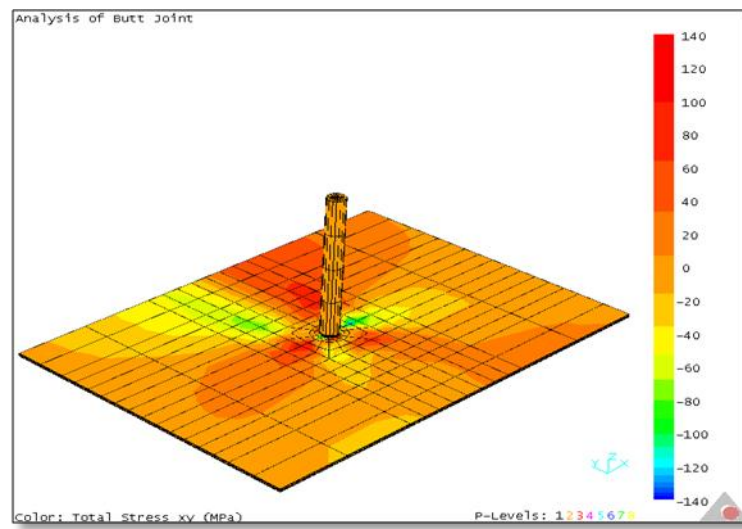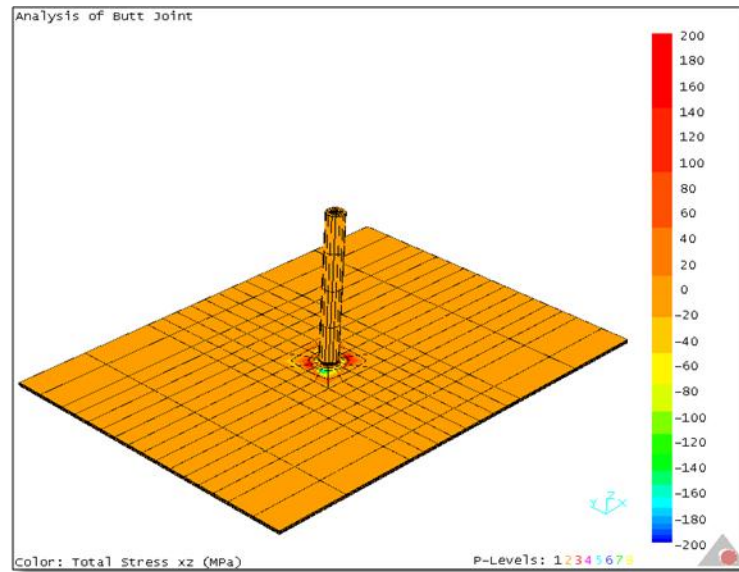welding for ω=1000 rpm and v=5 mm/s.

Figure 4.32 shows the temperature variation during FSW on x, y, z coordinate
plane coordinates (0;0;0), (0;10;0), (0;20;0), (0;30;0), (0;40;0) [mm].

Figure 4.32 Temperatures at different coordinates for ω= 1000 rpm and v= 5 mm/s

4.1.5 Pin rotational speed ω = 1200 rpm and pin transverse speed v = 2.5 mm/s

In this section, the finite element analyses were performed for pin rotational speed
of 1200 rpm and transverse speed of 2.5 mm/s. The welding conditions can be seen
in Table 4.5.

Table 4.5 Friction welding parameters of AA 6061 for ω= 1200 rpm and v = 2.5 mm/s

Pin Diameter (mm)	4
Pin Height (mm)	2.79
Tilt Angle (deg)	0
Pin Rotational Speed (rpm)	1200
Pin Translational Speed (rpm)	2.5
Shoulder Diameter (mm)	16
Shoulder Height (mm)	150
Reference Temperature (K)	293

Figure 4.33 shows the temperature distribution during the welding. As seen form the figure, temperature increases as the rotational speed increases compared to the results obtained by the analyses for 800 rpm and 1000 rpm. The maximum temperatures are 500 and 465 ^{o}C on the tool and plate, respectively.
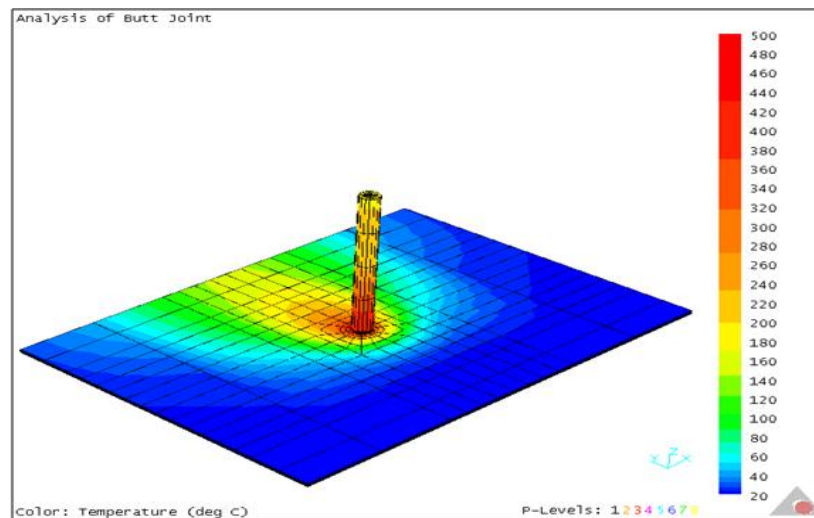
Figure 4.33 Temperature of AA 6061 for ω = 1200 rpm and v= 2.5 mm/s

Figures 4.34 - 4.39 present the stress distributions (σ_x, σ_y, σ_z, τ_{xy}, τ_{xz} and τ_{yz}) during the welding process.

Figure 4.34 σ_x stress distribution in the AA 6061 alloy plates during welding for ω=1200 rpm and v=2.5 mm/s.

Figure 4.35 σ_y stress distribution in the AA 6061 alloy plates during welding for ω=1200 rpm and v=2.5 mm/s.

Figure 4.36 σ_z stress distribution in the AA 6061 alloy plates during welding for ω=1200 rpm and v=2.5 mm/s.
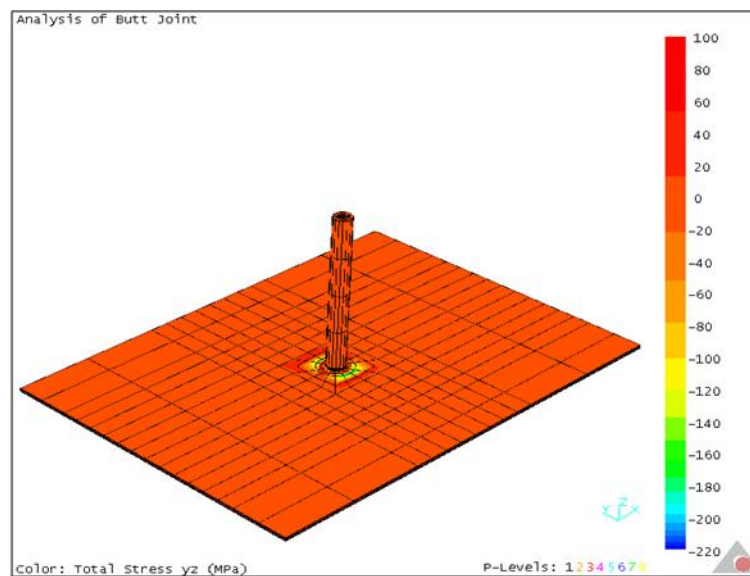

Figure 4.37 τ_{xy} stress distribution in the AA 6061 alloy plates during welding for ω=1200 rpm and v=2.5 mm/s.
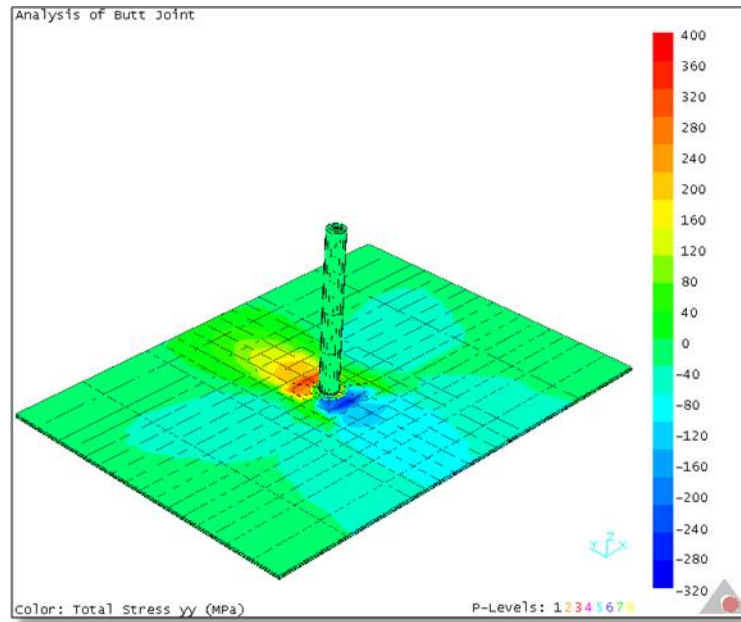
Figure 4.38 τ_{xz} stress distribution in the AA 6061 alloy plates during welding for ω=1200 rpm and v=2.5 mm/s.

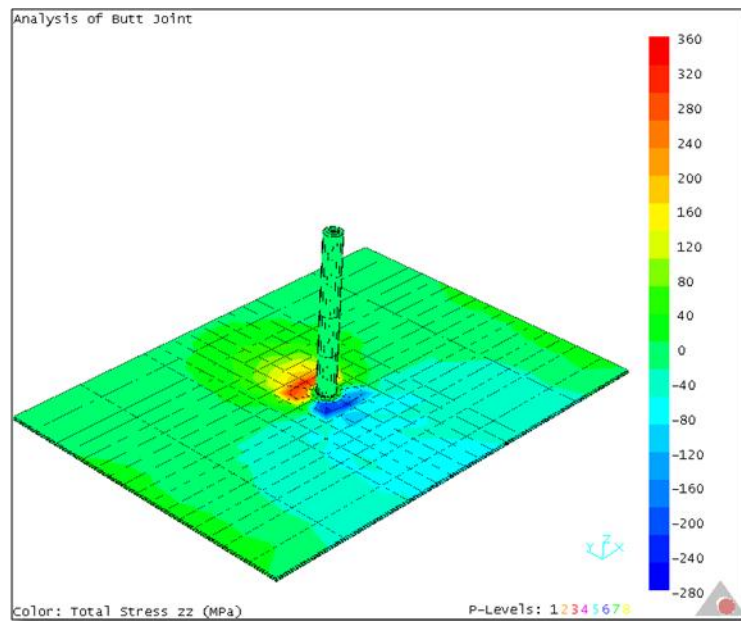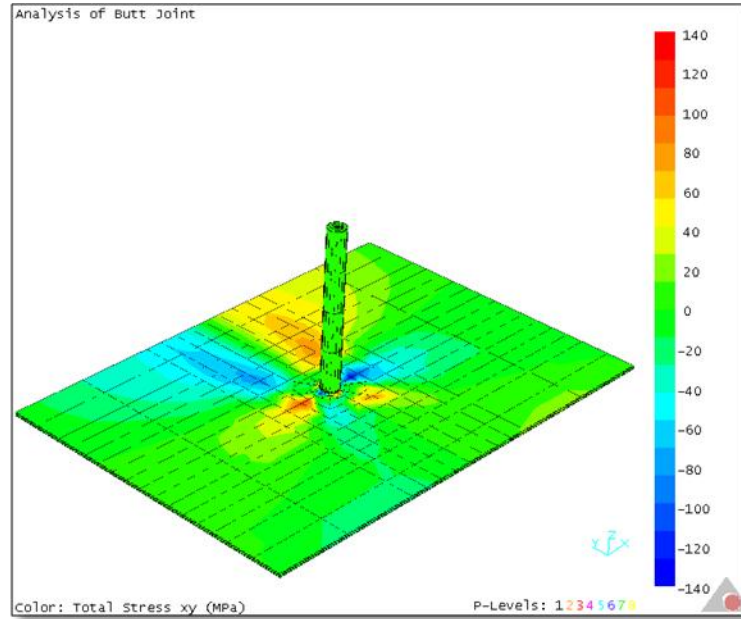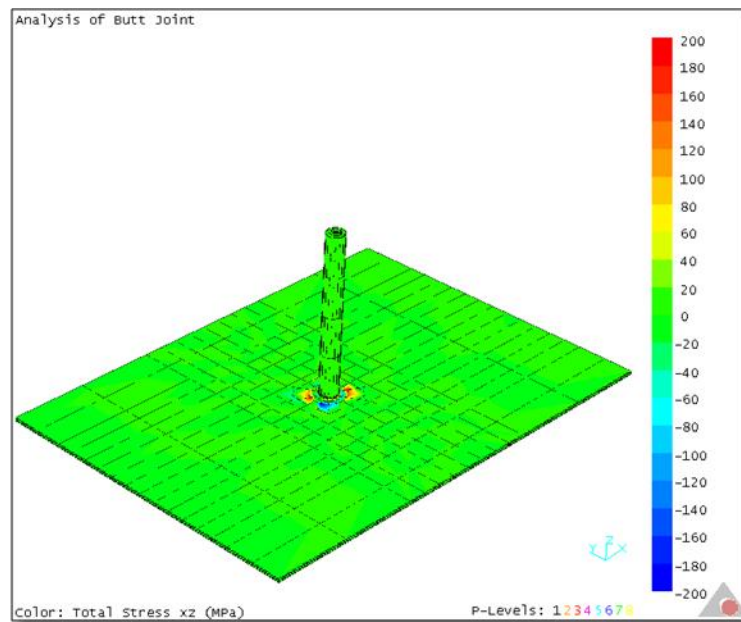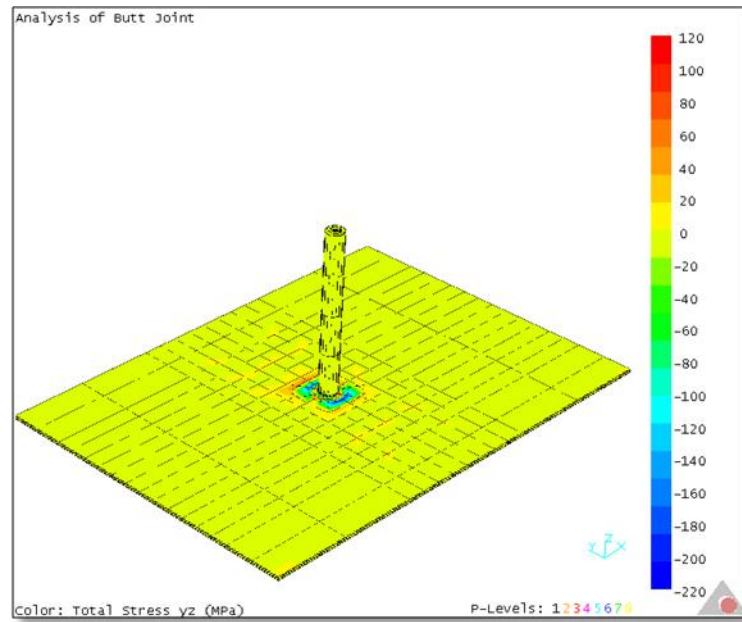Figure 4.39 τ_{yz} stress distribution in the AA 6061 alloy plates during welding for ω=1200 rpm and v=2.5 mm/s.

Figure 4.40 shows the temperature variation during FSW on x, y, z coordinate plane coordinates (0;0;0), (0;10;0), (0;20;0), (0;30;0), (0;40;0) [mm].
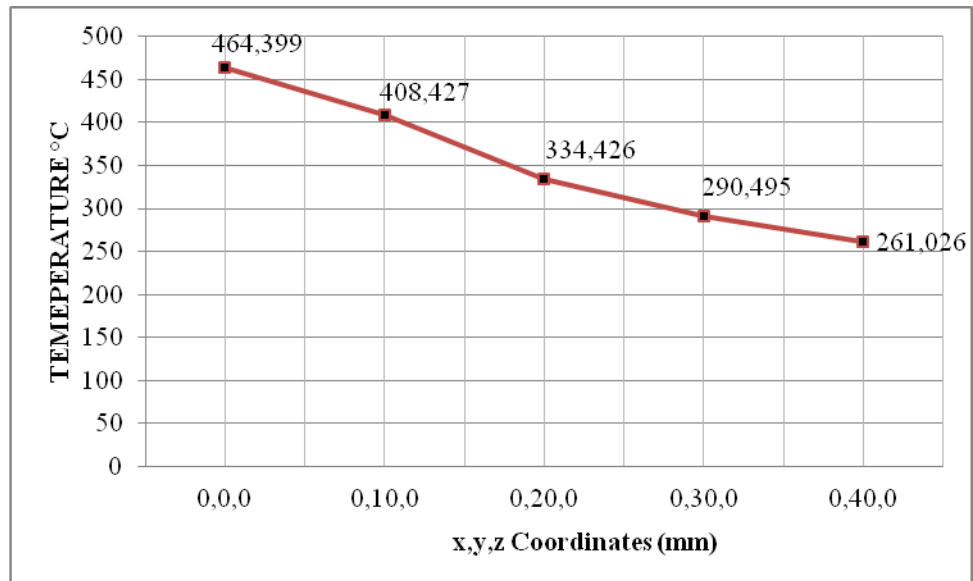
Figure 4.40 Temperatures at different coordinates for AA 6061 ω= 1200 rpm and v = 2.5 mm/s.

4.1.6 Pin rotational speed ω = 1200 rpm and pin transverse speed v = 5 mm/s

In this section, the finite element analyses were repeated for pin rotational speed of 1200 rpm and transverse speed of 5 mm/s. The welding conditions can be seen in Table 4.6.

Table 4.6 Friction welding parameters of AA 6061 for ω=344 rpm and v=5.5 mm/s

Pin Diameter (mm)	4
Pin Height (mm)	2.79
Tilt Angle (deg)	0
Pin Rotational Speed (rpm)	1200
Pin Translational Speed (rpm)	5
Shoulder Diameter (mm)	16
Shoulder Height (mm)	150
Reference Temperature (K)	293

Figure 4.41 shows the temperature distribution during the welding. The maximum temperatures are 480 and 460 ^{o}C on the tool and plate, respectively.
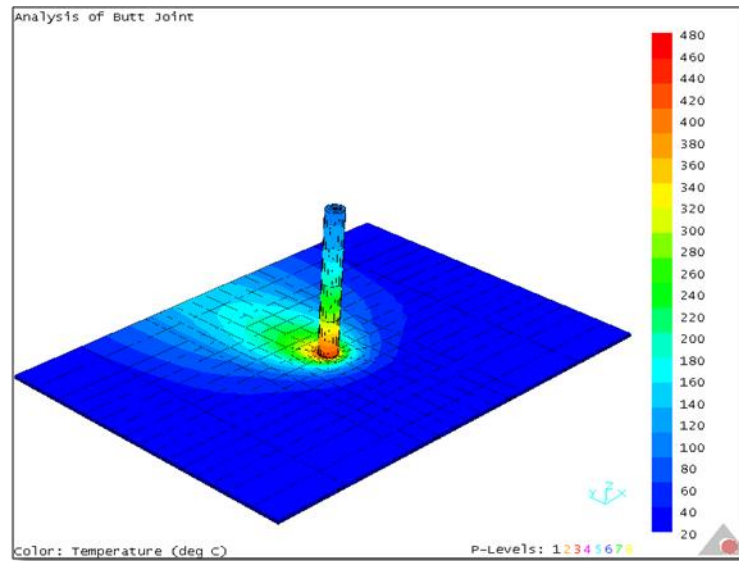
Figure 4.41 Temperature of AA 6061 for ω = 1200 rpm and v= 5 mm/s

Figures 4.42 - 4.47 present the stress distributions (σ_x, σ_y, σ_z, τ_{xy}, τ_{xz} and τ_{yz}) during the welding process.

Figure 4.42 σ_x stress distribution in the AA 6061 alloy plates during welding for ω=1200 rpm and v=5 mm/s.

Figure 4.43 σ_y stress distribution in the AA 6061 alloy plates during welding for ω=1200 rpm and v=5 mm/s.

Figure 4.44 σ_z stress distribution in the AA 6061 alloy plates during welding for ω=1200 rpm and v=5 mm/s.

Figure 4.45 τ_{xy} stress distribution in the AA 6061 alloy plates during welding for ω=1200 rpm and v=5 mm/s.

Figure 4.46 τ_{xz} stress distribution in the AA 6061 alloy plates during welding for ω=1200 rpm and v=5 mm/s.

Figure 4.47 τ_{yz} stress distribution in the AA 6061 alloy plates during welding for ω=1200 rpm and v=5 mm/s.

Figure 4.48 shows the temperature variation during FSW on x, y, z coordinate plane coordinates (0;0;0), (0;10;0), (0;20;0), (0;30;0), (0;40;0) [mm].
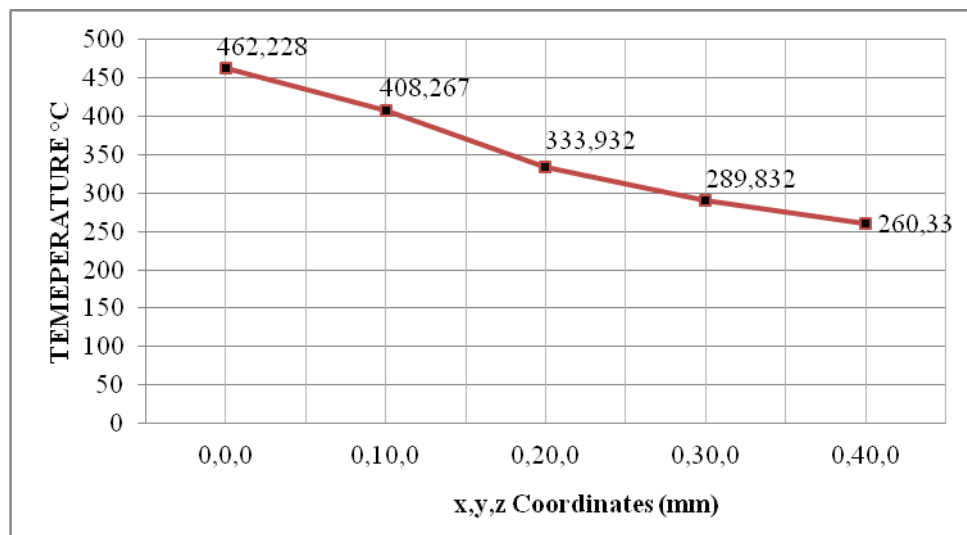
Figure 4.48 Temperatures at different coordinates for AA 6061 ω= 1200 rpm and v = 5 mm/s

4.2 AA 7075

Finite element analyses were repeated using AA 7075 for same welding conditions.

4.2.1 Pin rotational speed ω = 800 rpm and pin transverse speed v = 2.5 mm/s

Table 4.7 shows the welding conditions.

Table 4.7 Friction welding parameters of AA 7075 for ω= 800 rpm and v = 2.5 mm/s

Pin Diameter (mm)	4
Pin Height (mm)	2.79
Tilt Angle (deg)	0
Pin Rotational Speed (rpm)	800
Pin Translational Speed (rpm)	2.5
Shoulder Diameter (mm)	16
Shoulder Height (mm)	150
Reference Temperature (K)	293

The dimensions of the workpieces are shown in Fig. 4.49. Pin rotational speed and traverse speed are ω=800 rpm and v= 2.5 mm/s, respectively. The reference temperature is 20° C. Fig 4.48 shows the temperature distribution of the workpieces joined by FSW during welding.
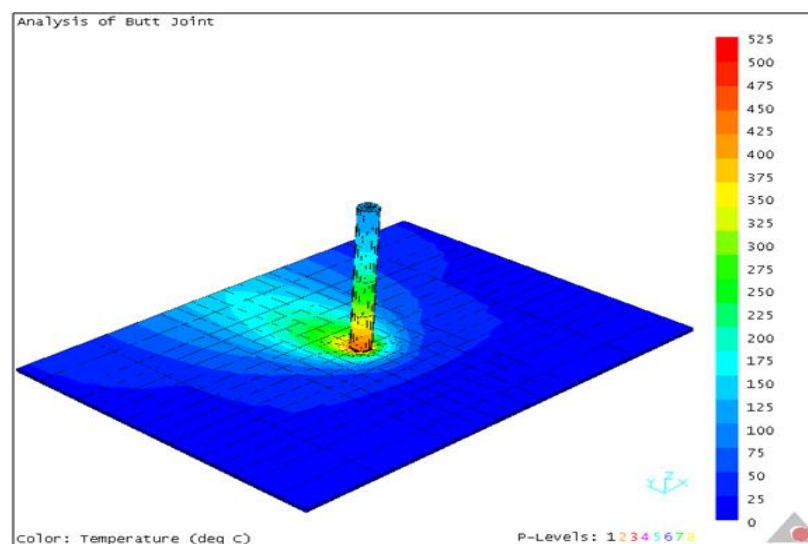
Figure 4.49 Temperature of AA 7075 for ω = 800 rpm and v = 2.5 mm/s

As shown in the figure, the maximum temperature reaches about 525 $^{\circ}$C on the tool. The maximum temperature of the plate is about 495 $^{\circ}$C. It can be seen that the temperature incerases significantly when AA 7075 plate is used.

Fig 4.50 - 4.55 present the stress distributions (σ_x, σ_y, σ_z, τ_{xy}, τ_{xz} and τ_{yz}) during the welding process.

Figure 4.50 σ_x stress distribution in the AA 7075 alloy plates during welding for ω=800 rpm and v=2.5 mm/s.
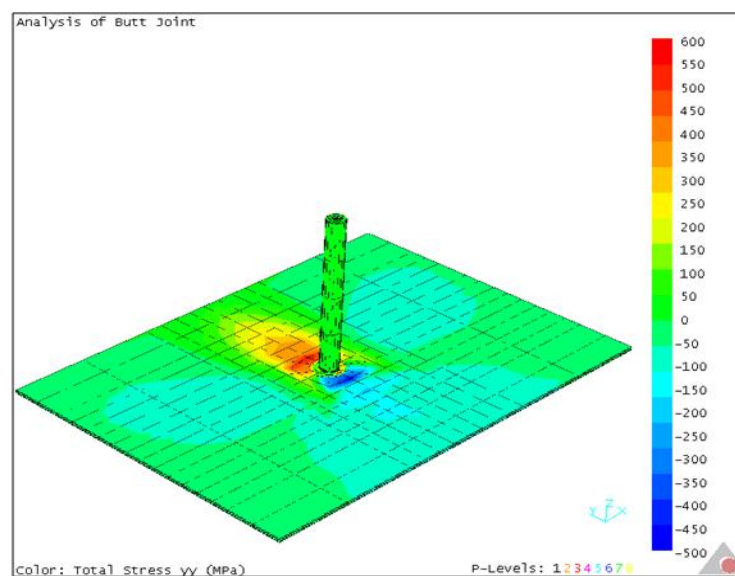
Figure 4.51 σ_y stress distribution in the AA 7075 alloy plates during welding for ω=800 rpm and v= 2.5 mm/s.
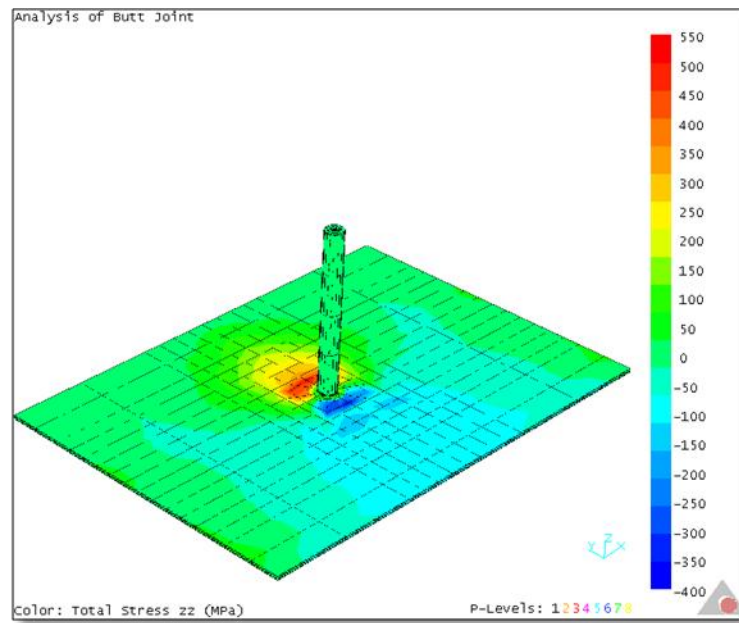
Figure 4.52 σ_z stress distribution in the AA 7075 alloy plates during welding for ω=800 rpm and v= 2.5 mm/s.
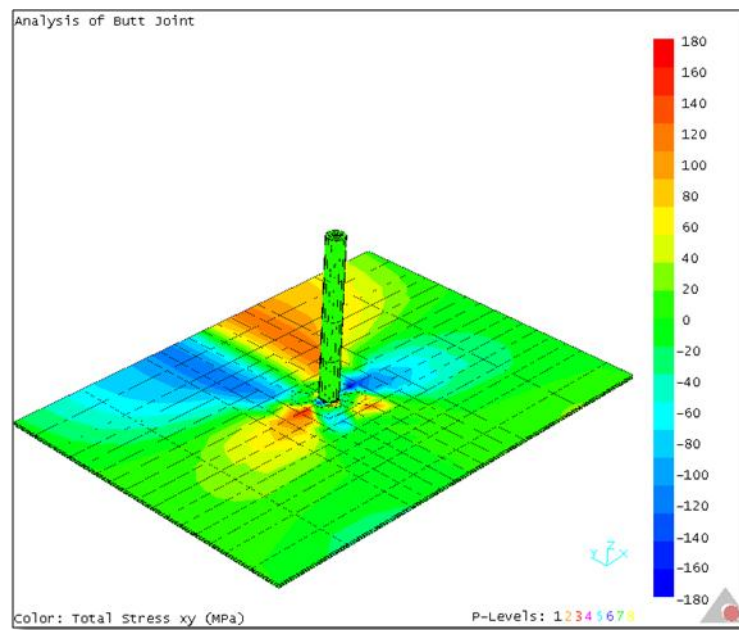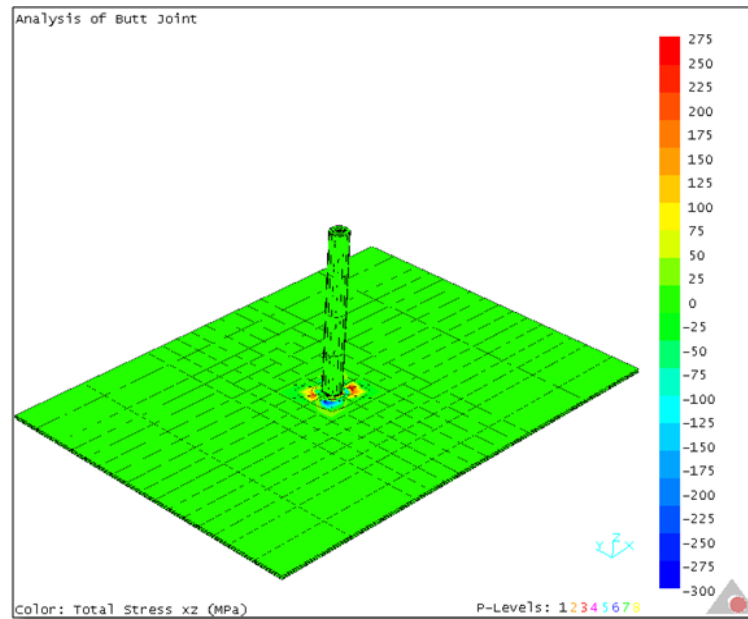

Figure 4.53 τ_{xy} stress distribution in the AA 7075 alloy plates during welding for ω=800 rpm and v= 2.5 mm/s.
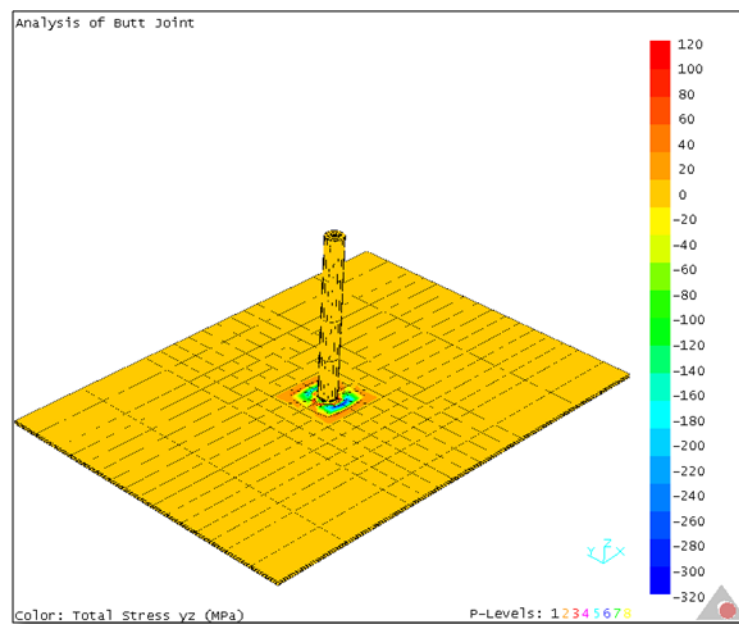
Figure 4.54 τ_{xz} stress distribution in the AA 7075 alloy plates during welding for ω=800 rpm and v= 2.5 mm/s.

Figure 4.55 τ_{yz} stress distribution in the AA 7075 alloy plates during welding for ω=800 rpm and v= 2.5 mm/s.

Figure 4.56 show the temperature variation during FSW on x, y, z coordinate plane coordinates (0;0;0), (0;10;0), (0;20;0), (0;30;0), (0;40;0) [mm].
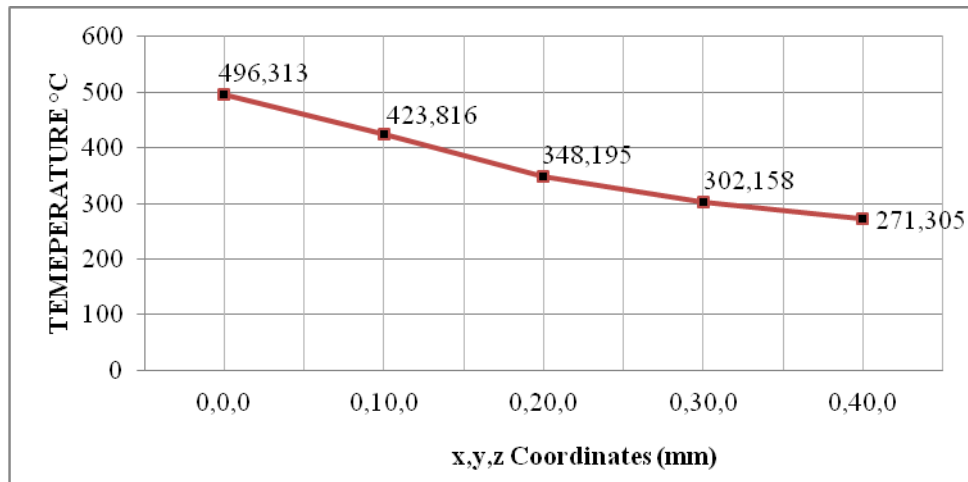
Figure 4.56 Temperatures at different coordinates for ω= 800 rpm and v = 2.5 mm/s

4.2.2 Pin rotational speed ω = 800 rpm and pin transverse speed v = 5 mm/s

In this section, the finite element analyses were performed for pin rotational speed of 800 rpm and transverse speed of 5 mm/s. The welding conditions can be seen in Table 4.8.

Table 4.8 Friction welding parameters of AA 7075 for ω= 800 rpm and v= 5 mm/s

Pin Diameter (mm)	4
Pin Height (mm)	2.79
Tilt Angle (deg)	0
Pin Rotational Speed (rpm)	800
Pin Translational Speed (rpm)	5
Shoulder Diameter (mm)	16
Shoulder Height (mm)	150
Reference Temperature (K)	293

Figure 4.57 shows the temperature distribution during the welding. The maximum temperatures are about 520 and 490 ^{o}C on the tool and plate, respectively. As seen from the figure the temperature decreases since the transverse speed increases.
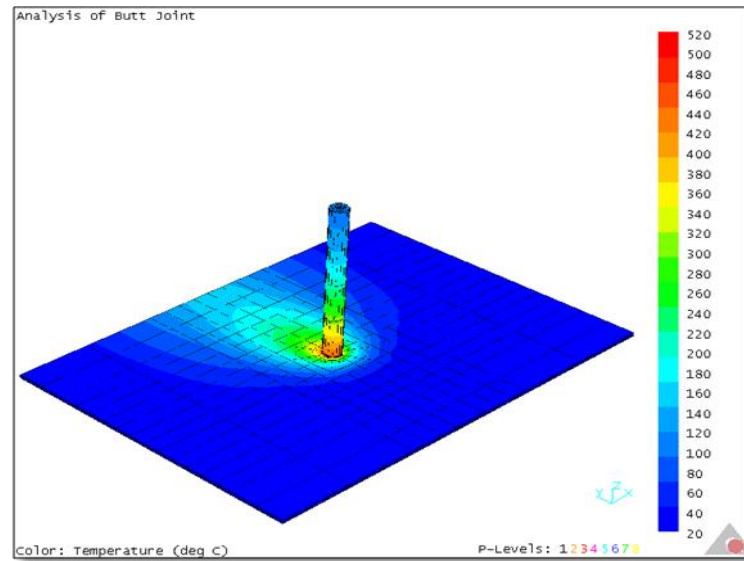
Figure 4.57 Temperature distribution in welded AA 7075 plates

for ω= 800 rpm and v= 5 mm/s

Figures 4.58 - 4.63 present the stress distributions (σ_x, σ_y, σ_z, τ_{xy}, τ_{xz} and τ_{yz}) during the welding process.
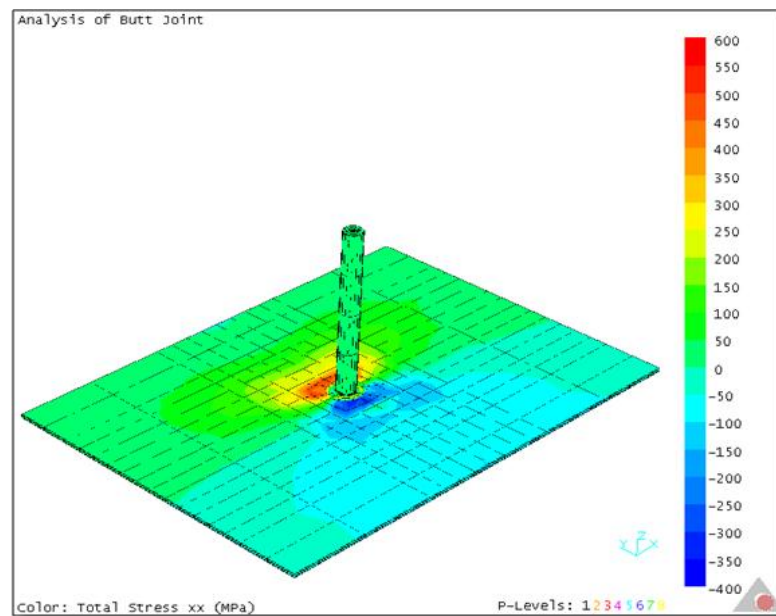

Figure 4.58 σ_x stress distribution in the AA 7075 alloy plates during

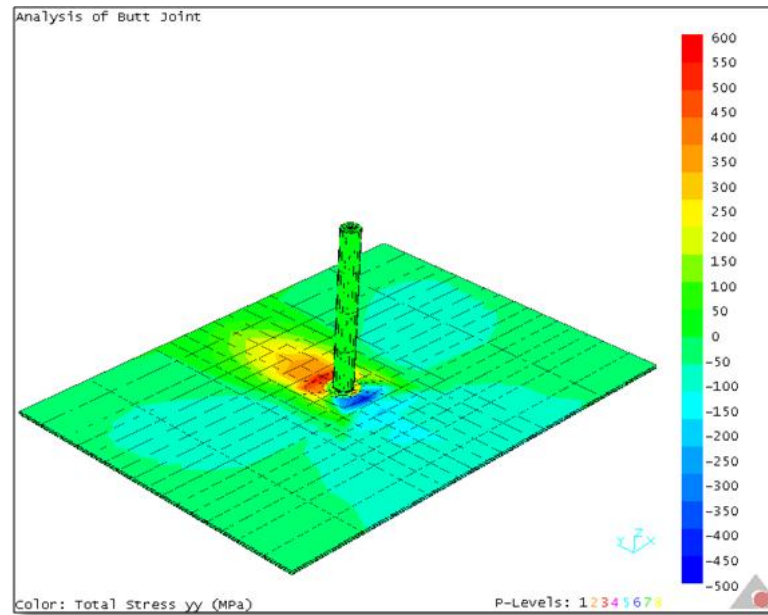welding for ω=800 rpm and v=5 mm/s.

Figure 4.59 σ_y stress distribution in the AA 7075 alloy plates during welding for ω=800 rpm and v=5 mm/s.
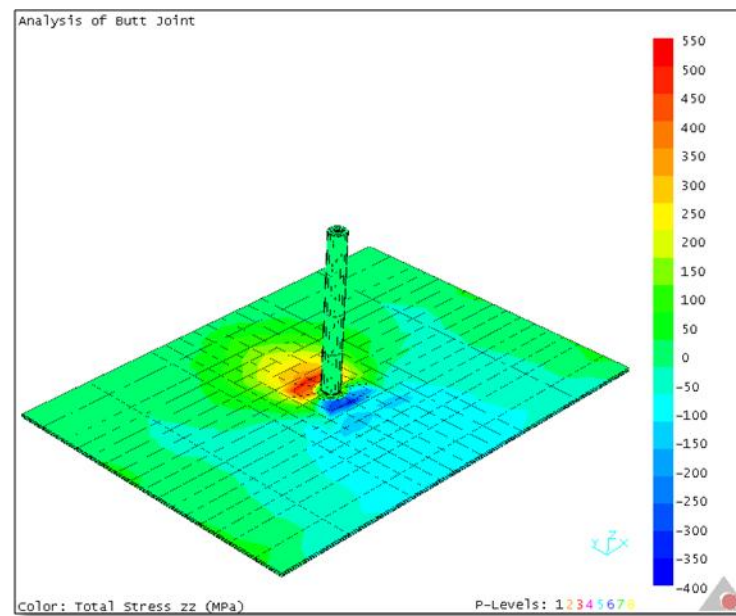

Figure 4.60 σ_z stress distribution in the AA 7075 alloy plates during welding for ω=800 rpm and v=5 mm/s.
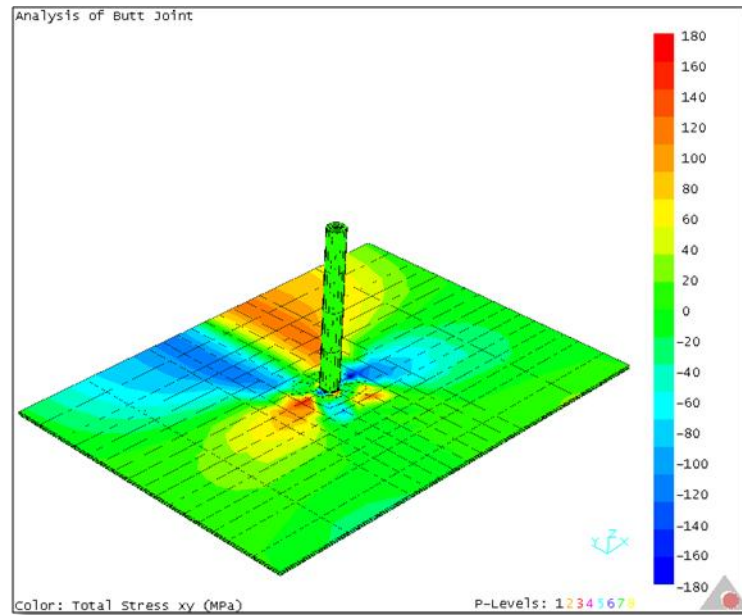
Figure 4.61 τ_{xy} stress distribution in the AA 7075 alloy plates during welding for ω=800 rpm and v=5 mm/s.
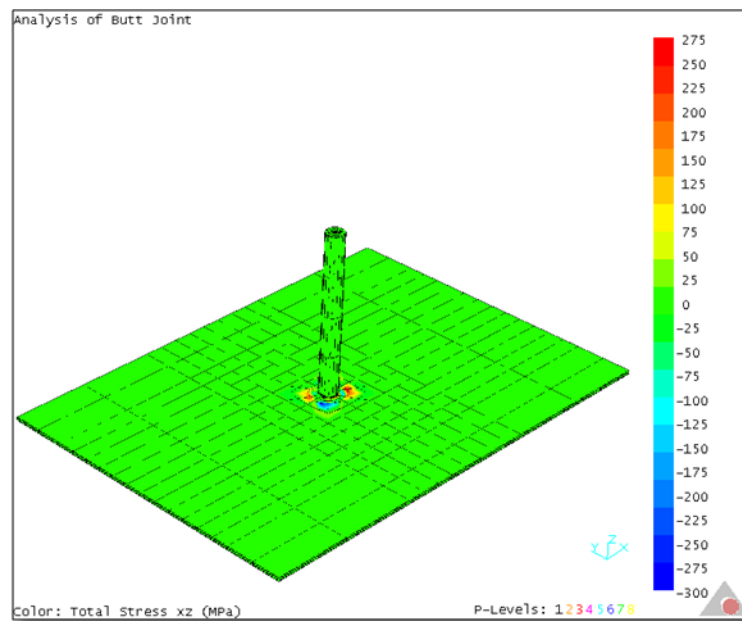

Figure 4.62 τ_{xz} stress distribution in the AA 7075 alloy plates during welding for ω=800 rpm and v=5 mm/s.
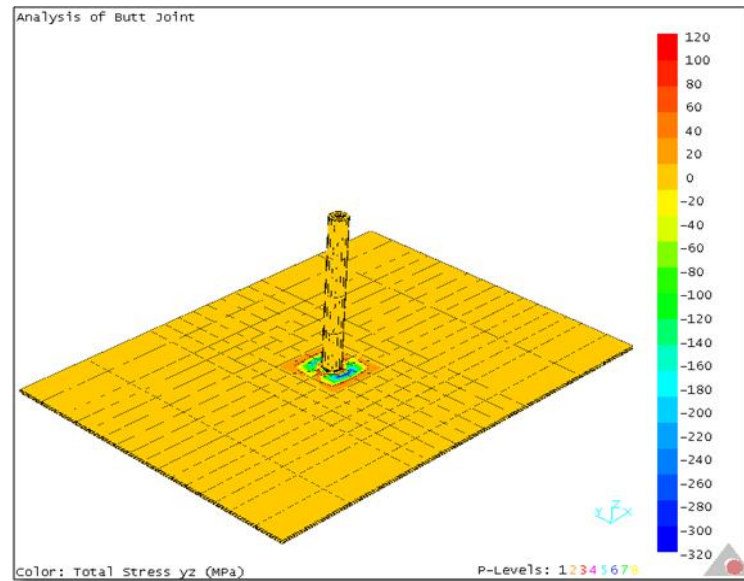
Figure 4.63 τ_{yz} stress distribution in the AA 7075 alloy plates during
welding for ω=800 rpm and v=5 mm/s.

Figure 4.64 shows the temperature variation during FSW on x, y, z coordinate plane coordinates (0;0;0), (0;10;0), (0;20;0), (0;30;0), (0;40;0) [mm].
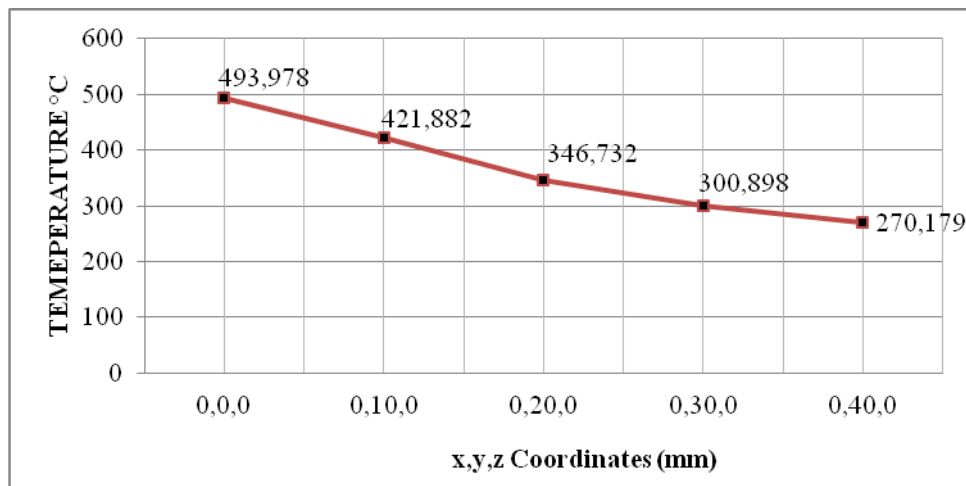

Figure 4.64 Temperatures at different coordinates for ω= 800 rpm and v = 5 mm/s

4.2.3 Pin rotational speed ω = 1000 rpm and pin transverse speed v = 2.5 mm/s

In order to determine the effect of the pin rotational speed, the finite element analyses were repeated for the rotational speeds of 1000 rpm. Table 4.9 presents this weld conditions.

Table 4.9 Friction welding parameters of AA 7075 for ω = 1000 rpm and v=2.5 mm/s

Pin Diameter (mm)	4
Pin Height (mm)	2.79
Tilt Angle (deg)	0
Pin Rotational Speed (rpm)	1000
Pin Translational Speed (rpm)	2.5
Shoulder Diameter (mm)	16
Shoulder Height (mm)	150
Reference Temperature (K)	293

Figure 4.65 shows the temperature distribution during the welding. As seen form the figure, temperature increases as the rotational speed increases compared to the results obtained by the analyses for 800 rpm. The maximum temperatures are 575 and 540 ^{o}C on the tool and plate, respectively.
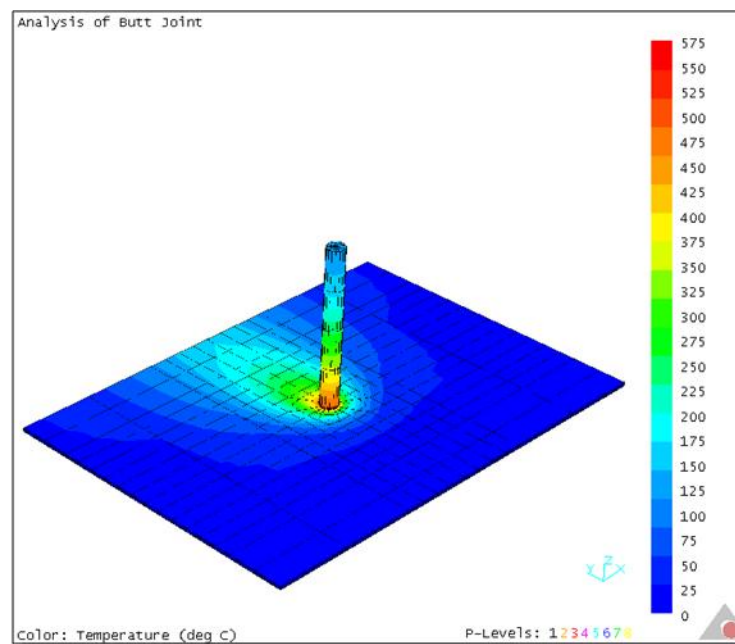
Figure 4.65 Tempeature of AA 7075 w= 1000 rpm V= 2.5 mm/s

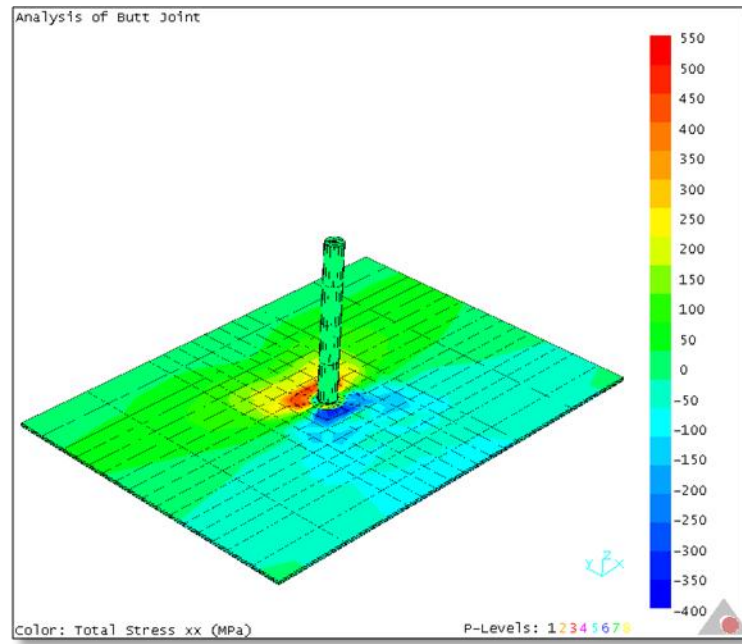Figures 4.66 - 4.71 show the stress distributions during the welding process for 1000 rpm.

Figure 4.66 σ_x stress distribution in the AA 7075 alloy plates during welding for ω=1000 rpm and v=2.5 mm/s.
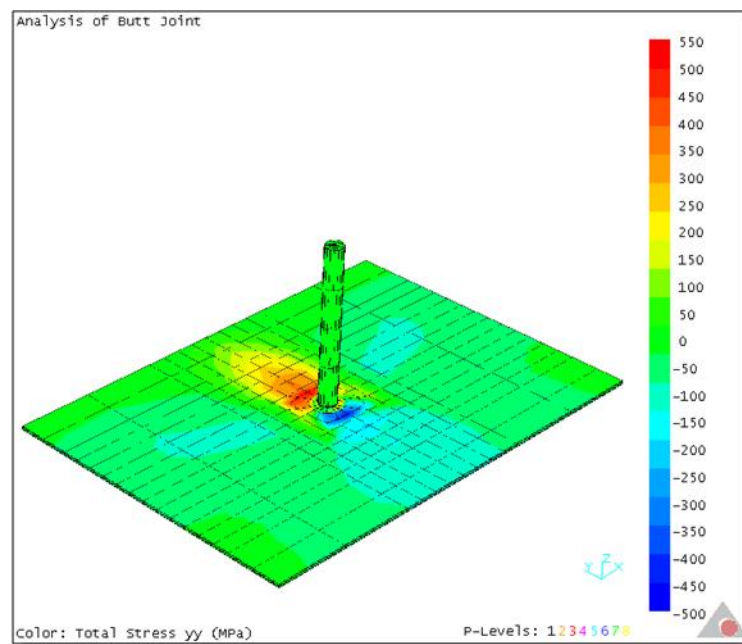

Figure 4.67 σ_y stress distribution in the AA 7075 alloy plates during welding for ω=1000 rpm and v=2.5 mm/s.

Figure 4.68 σ_z stress distribution in the AA 7075 alloy plates during welding for ω=1000 rpm and v=2.5 mm/s.

Figure 4.69 τ_{xy} stress distribution in the AA 7075 alloy plates during welding for ω=1000 rpm and v=2.5 mm/s.

Figure 4.70 τ_{xz} stress distribution in the AA 7075 alloy plates during welding for ω=1000 rpm and v=2.5 mm/s.

Figure 4.71 τ_{yz} stress distribution in the AA 7075 alloy plates during welding for ω=1000 rpm and v=2.5 mm/s.
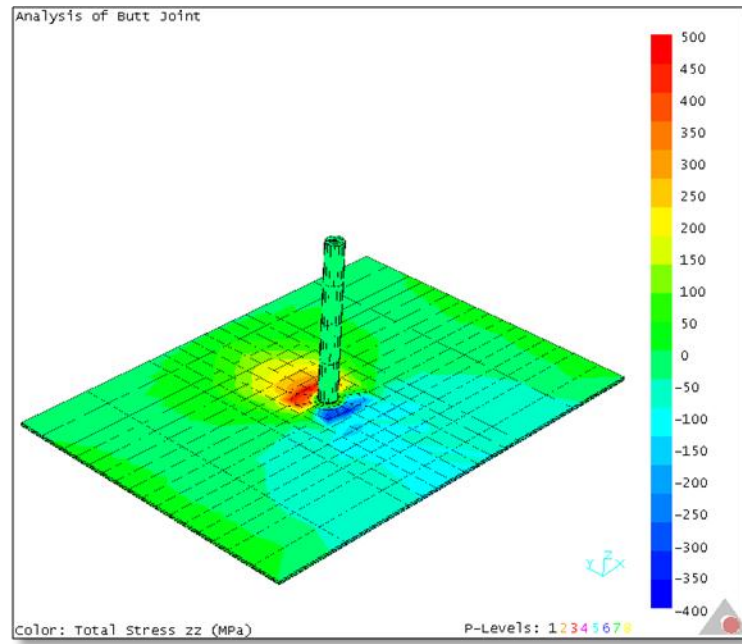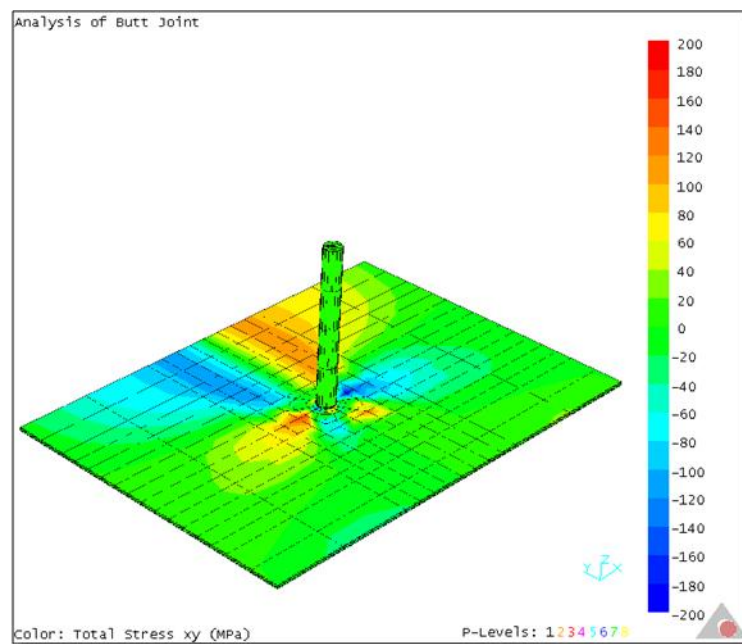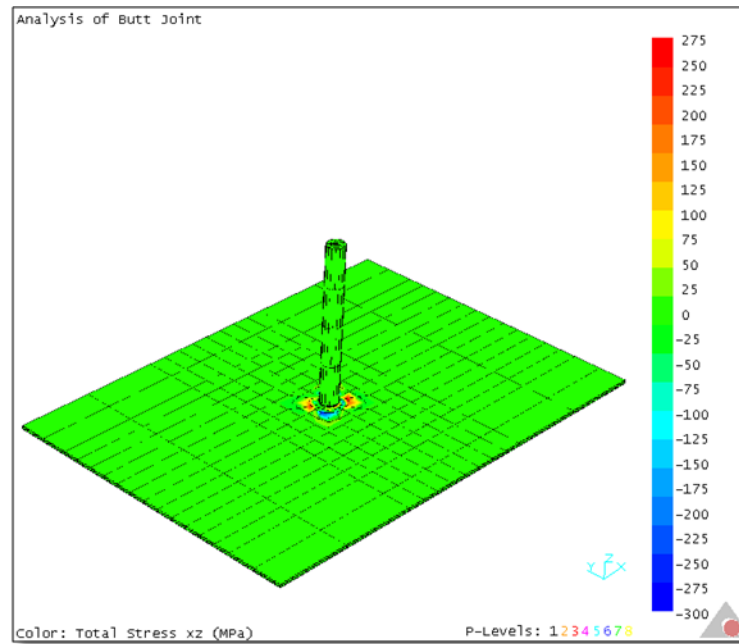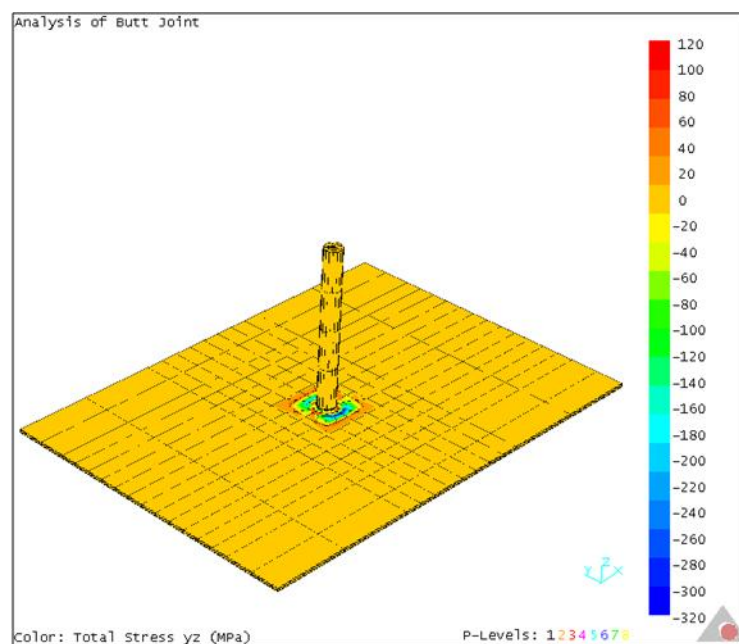
Figure 4.72 show the temperature variation during FSW on x, y, z coordinate plane coordinates (0;0;0), (0;10;0), (0;20;0), (0;30;0), (0;40;0) [mm].
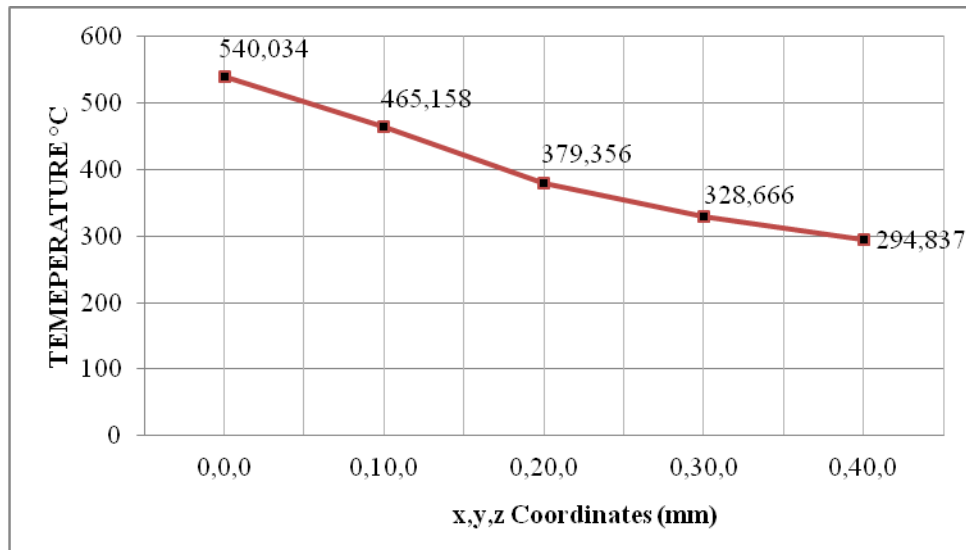
Figure 4.72 Temperatures at different coordinates for ω= 1000 rpm and v = 2.5 mm/s

4.2.4 Pin rotational speed ω = 1000 rpm and pin transverse speed v = 5 mm/s

In this section, the finite element analyses were performed for pin rotational speed of 1000 rpm and transverse speed of 5 mm/s. The welding conditions can be seen in Table 4.10.

Table 4.10 Friction welding parameters of AA 7075 for ω= 1000 rpm and v=5 mm/s

Pin Diameter (mm)	4
Pin Height (mm)	2.79
Tilt Angle (deg)	0
Pin Rotational Speed (rpm)	1000
Pin Translational Speed (rpm)	5
Shoulder Diameter (mm)	16
Shoulder Height (mm)	150
Reference Temperature (K)	293

Figure 4.73 shows the temperature distribution during the welding. The maximum temperatures are about 575 and 538 ^{o}C on the tool and plate, respectively. As seen from the figure the temperature decreases since the transverse speed increases.
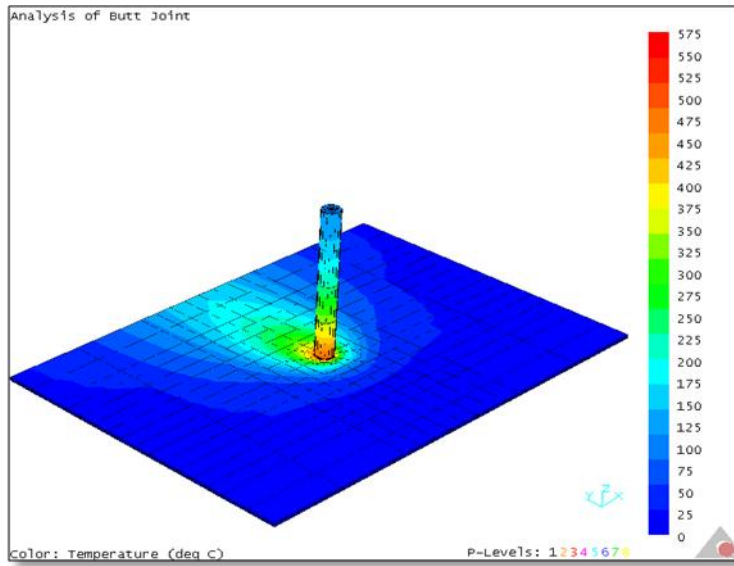
Figure 4.73 Temperature of AA 7075 w= 1000 rpm V= 5 mm/s

Figures 4.74 - 4.79 present the stress distributions (σ_x, σ_y, σ_z, τ_{xy}, τ_{xz} and τ_{yz}) during the welding process.

Figure 4.74 σ_x stress distribution in the AA 7075 alloy plates during welding for ω=1000 rpm and v=5 mm/s.

Figure 4.75 σ_y stress distribution in the AA 7075 alloy plates during welding for ω=1000 rpm and v=5 mm/s.

Figure 4.76 σ_z stress distribution in the AA 7075 alloy plates during welding for ω=1000 rpm and v=5 mm/s.

Figure 4.77 τ_{xy} stress distribution in the AA 7075 alloy plates during welding for ω=1000 rpm and v=5 mm/s.
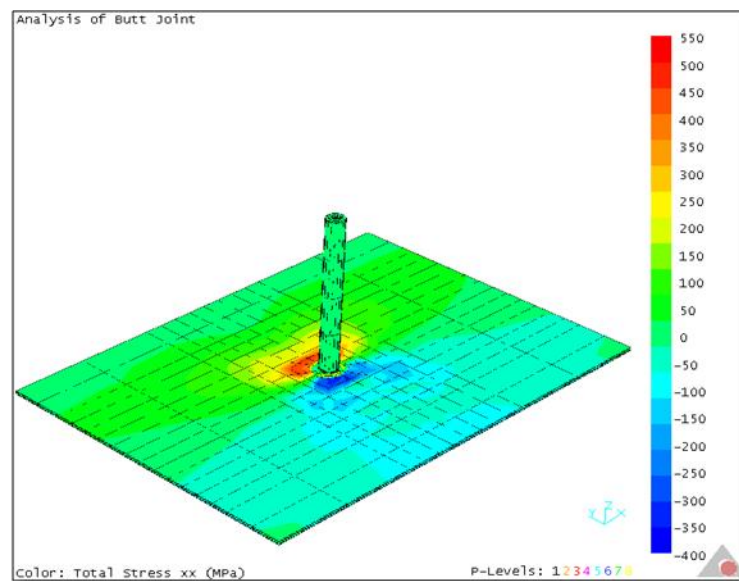

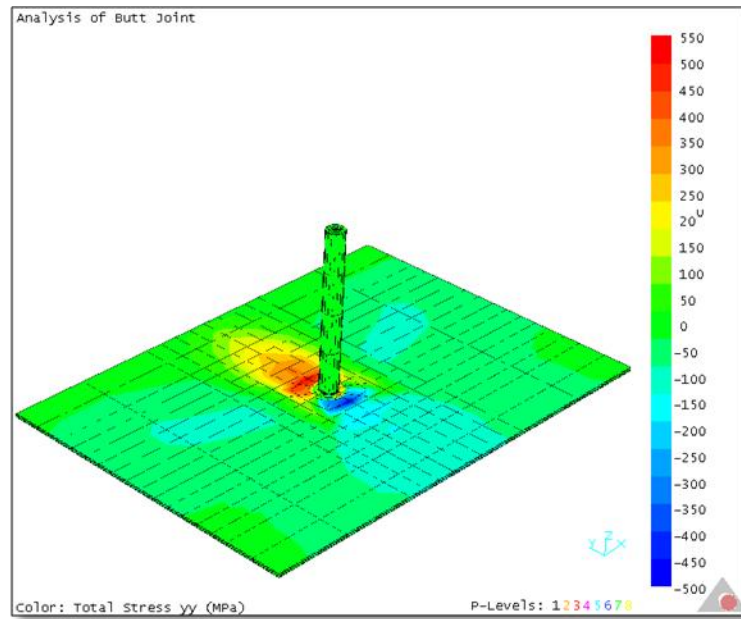Figure 4.78 τ_{xz} stress distribution in the AA 7075 alloy plates during welding for ω=1000 rpm and v=5 mm/s.

Figure 4.79 τ_{yz} stress distribution in the AA 7075 alloy plates during welding for ω=1000 rpm and v=5 mm/s.
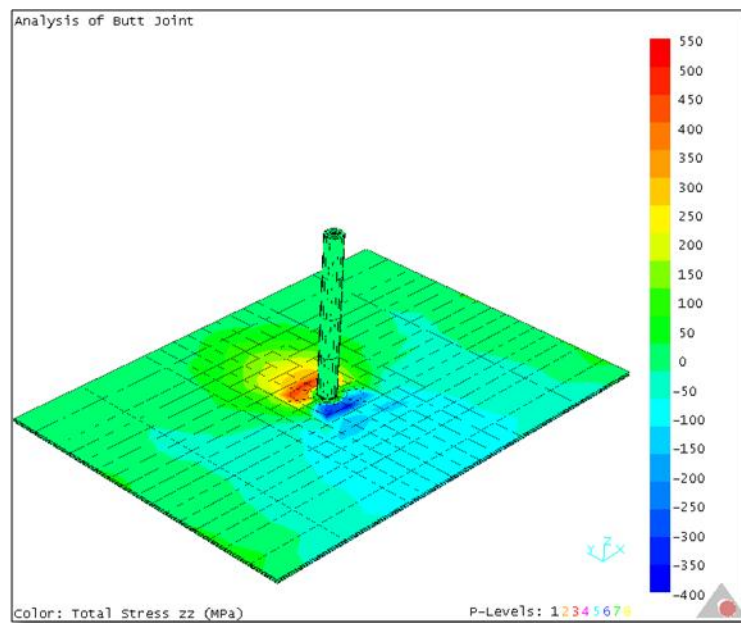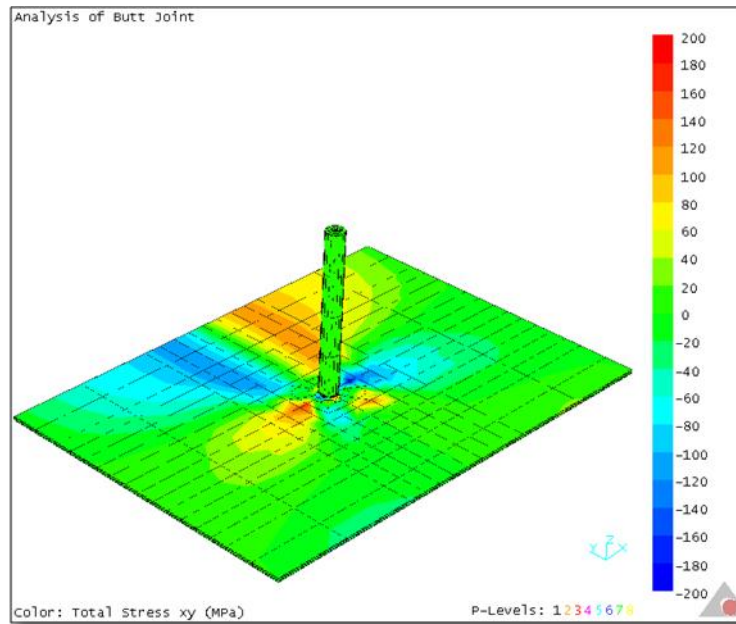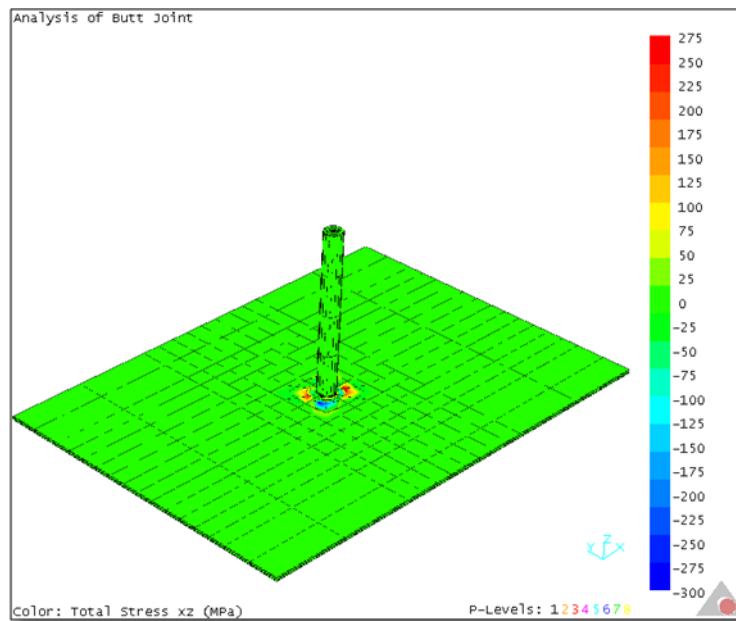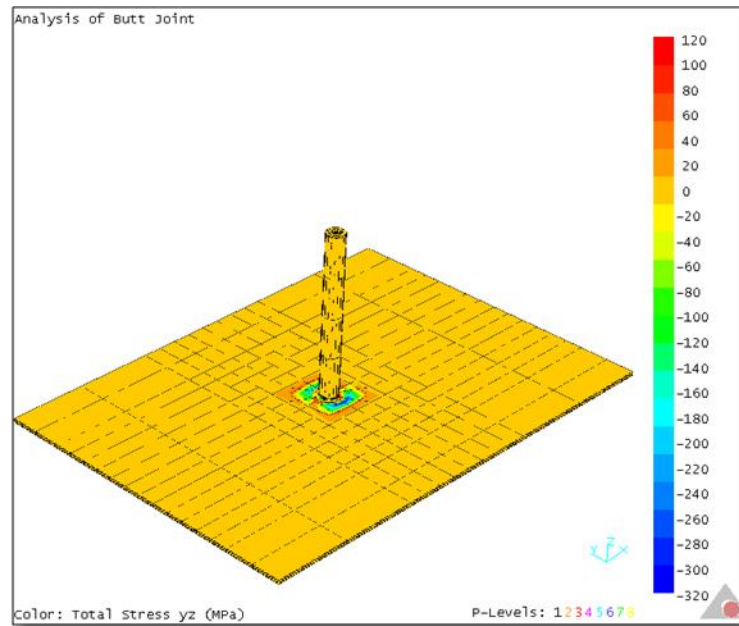
Figure 4.80 shows the temperature variation during FSW on x, y, z coordinate plane coordinates (0;0;0), (0;10;0), (0;20;0), (0;30;0), (0;40;0) [mm].
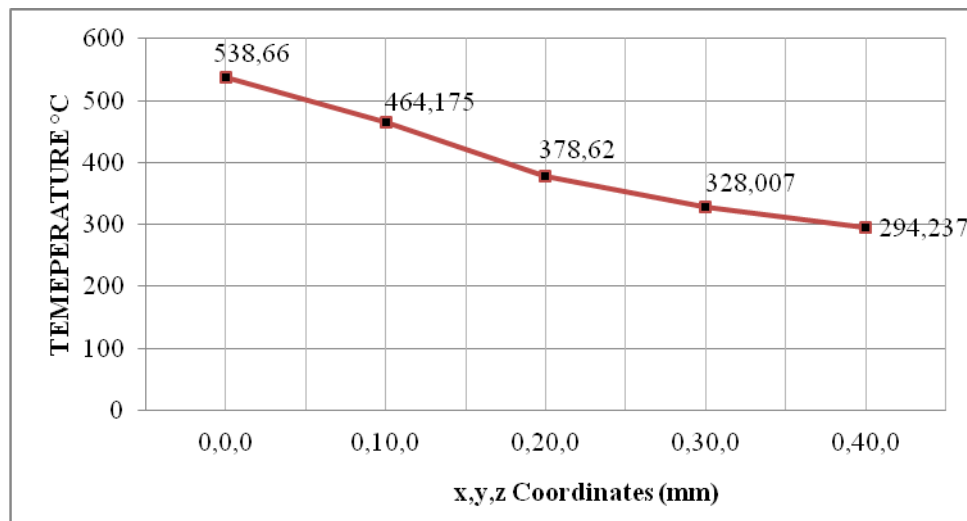

Figure 4.80Temperatures at different coordinates for ω= 1000 rpm and v= 5 mm/s

4.2.5 Pin rotational speed ω = 1200 rpm and pin transverse speed v = 2.5 mm/s

In this section, the finite element analyses were performed for pin rotational speed of 1200 rpm and transverse speed of 2.5 mm/s. The welding conditions can be seen in Table 4.11.

Table 4.11 Friction welding parameters of AA 7075 for ω= 1200 rpm and v = 2.5 mm/s

Pin Diameter (mm)	4
Pin Height (mm)	2.79
Tilt Angle (deg)	0
Pin Rotational Speed (rpm)	1200
Pin Translational Speed (rpm)	2,5
Shoulder Diameter (mm)	16
Shoulder Height (mm)	150
Reference Temperature (K)	293

Figure 4.81 shows the temperature distribution during the welding. As seen form the figure, temperature increases as the rotational speed increases compared to the results obtained by the analyses for 800 rpm and 1000 rpm. The maximum temperatures are 640 and 585 ^{o}C on the tool and plate, respectively.
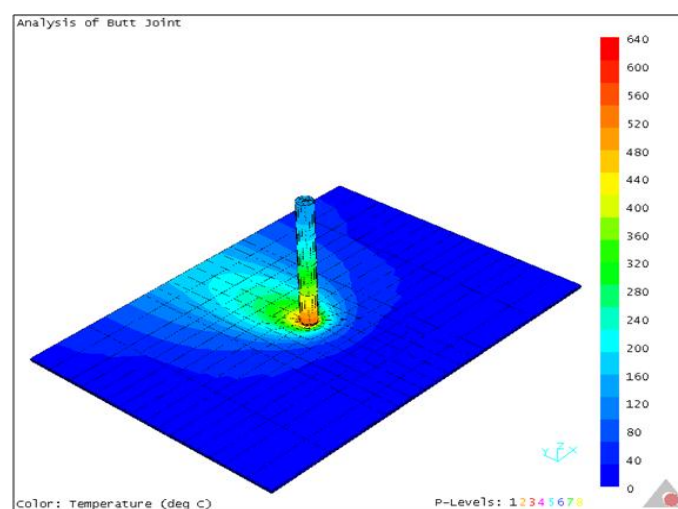
Figure 4.81 Temperature of AA 7075 for ω = 1200 rpm and

v= 2.5 mm/s

Figures 4.82 - 4.87 present the stress distributions (σ_x, σ_y, σ_z, τ_{xy}, τ_{xz} and τ_{yz}) during the welding process.

Figure 4.82 σ_x stress distribution in the AA 7075 alloy plates during welding for ω=1200 rpm and v=2.5 mm/s.

Figure 4.83 σ_y stress distribution in the AA 7075 alloy plates during welding for ω=1200 rpm and v=2.5 mm/s.

Figure 4.84 σ_z stress distribution in the AA 7075 alloy plates during welding for ω=1200 rpm and v=2.5 mm/s.

Figure 4.85 τ_{xy} stress distribution in the AA 7075 alloy plates during welding for ω=1200 rpm and v=2.5 mm/s.

Figure 4.86 τ_{xz} stress distribution in the AA 7075 alloy plates during welding for ω=1200 rpm and v=2.5 mm/s.

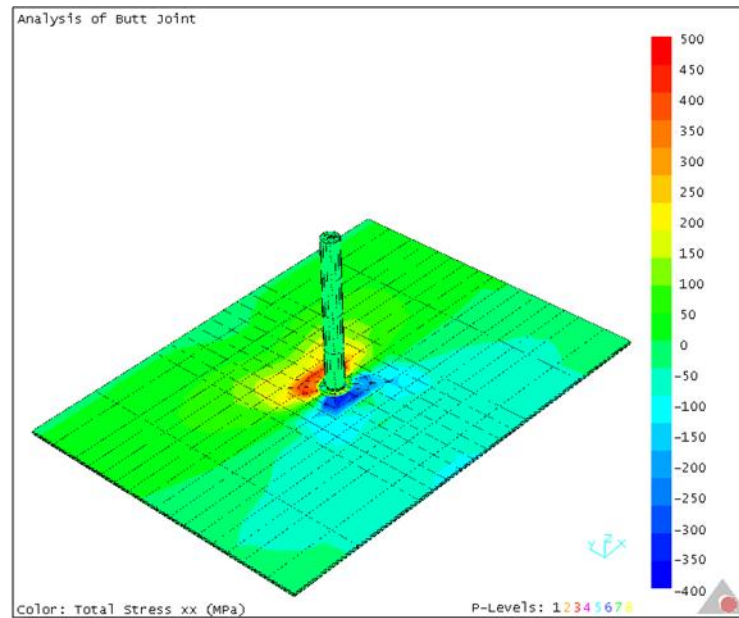Figure 4.87 τ_{yz} stress distribution in the AA 7075 alloy plates during welding for ω=1200 rpm and v=2.5 mm/s.

Figure 4.88 shows the temperature variation during FSW on x, y, z coordinate plane coordinates (0;0;0), (0;10;0), (0;20;0), (0;30;0), (0;40;0) [mm].

Figure 4.88 Temperatures at different coordinates for AA 7075 ω= 1200 rpm and v= 2.5 mm/s

4.2.6 Pin rotational speed ω = 1200 rpm and pin transverse speed v = 5 mm/s

In this section, the finite element analyses were repeated for pin rotational speed of 1200 rpm and transverse speed of 5 mm/s. The welding conditions can be seen in Table 4.12.

Table 4.12 Friction welding parameters of AA 7075 for ω=344 rpm and v=5.5 mm/s

Pin Diameter (mm)	4
Pin Height (mm)	2.79
Tilt Angle (deg)	0
Pin Rotational Speed (rpm)	1200
Pin Translational Speed (rpm)	5
Shoulder Diameter (mm)	16
Shoulder Height (mm)	150
Reference Temperature (K)	293

Figure 4.89 shows the temperature distribution during the welding. The maximum temperatures are 640 and 585 ^{o}C on the tool and plate, respectively.
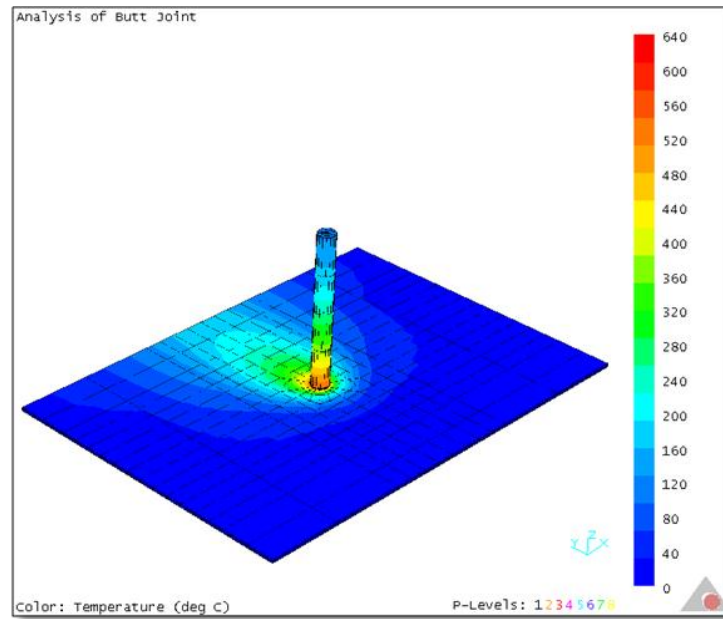
Figure 4.89 Temperature of AA 7075 for ω = 1200 rpm and v= 5 mm/s

Figures 4.90 - 4.95 present the stress distributions (σ_x, σ_y, σ_z, τ_{xy}, τ_{xz} and τ_{yz}) during the welding process.

Figure 4.90 σ_x stress distribution in the AA 7075 alloy plates during welding for ω=1200 rpm and v=5 mm/s.
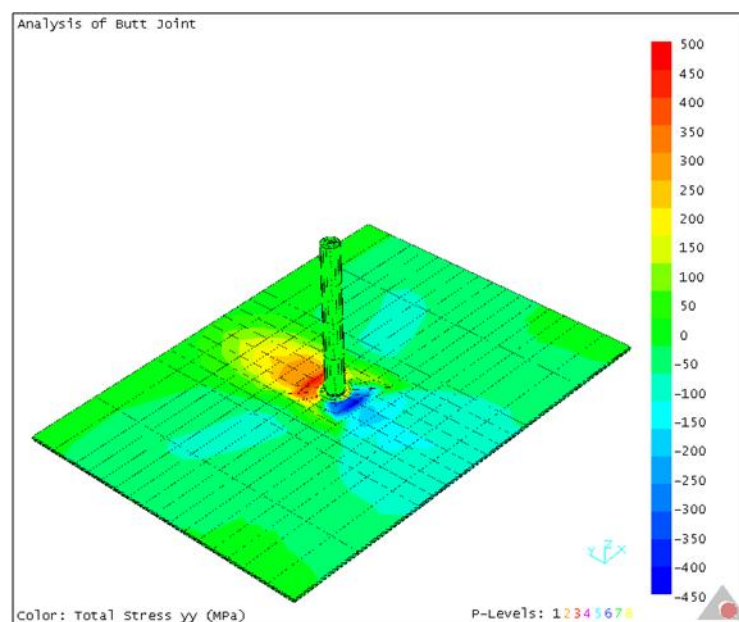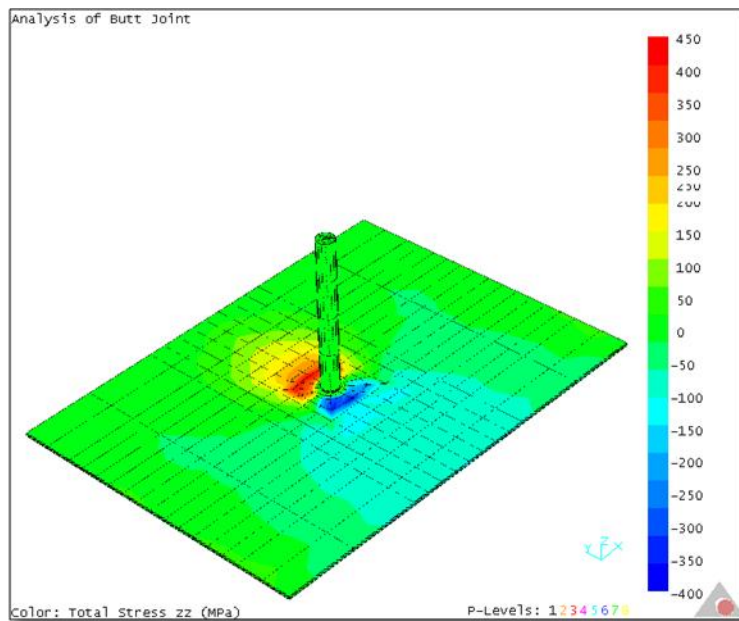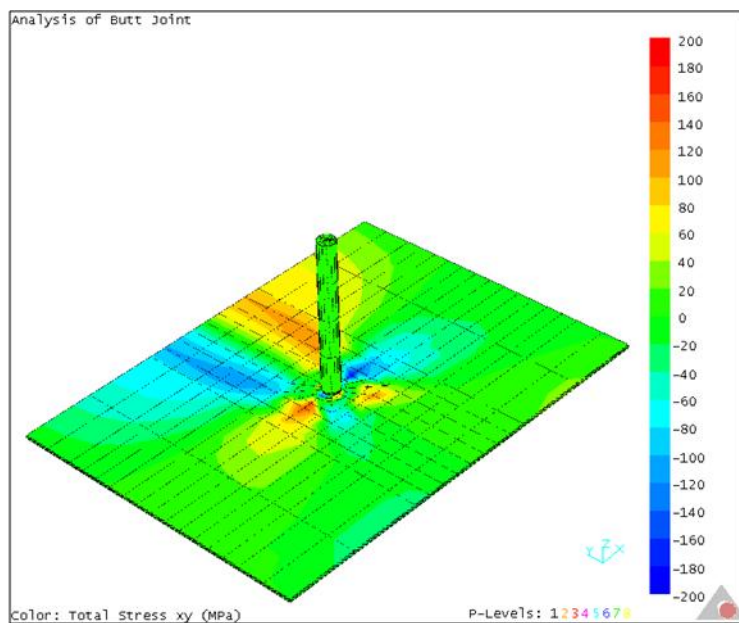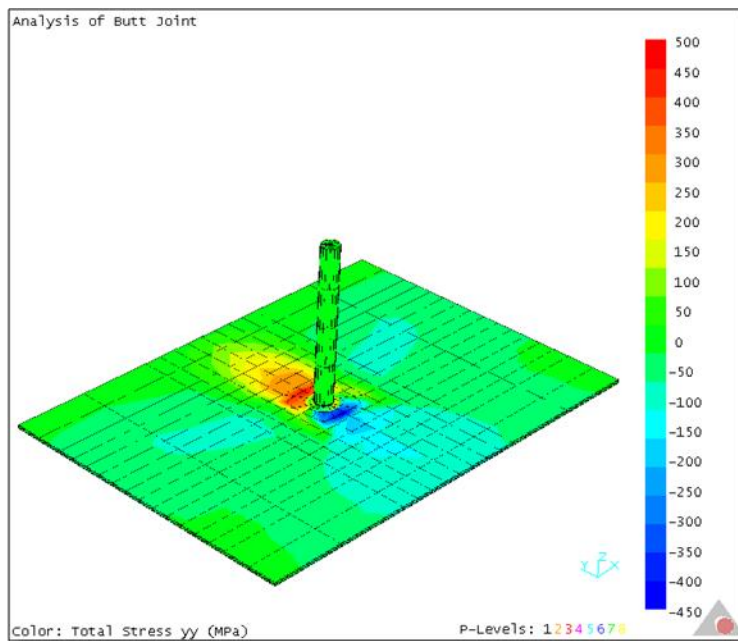
Figure 4.91 σ_y stress distribution in the AA 7075 alloy plates during welding for ω=1200 rpm and v=5 mm/s.
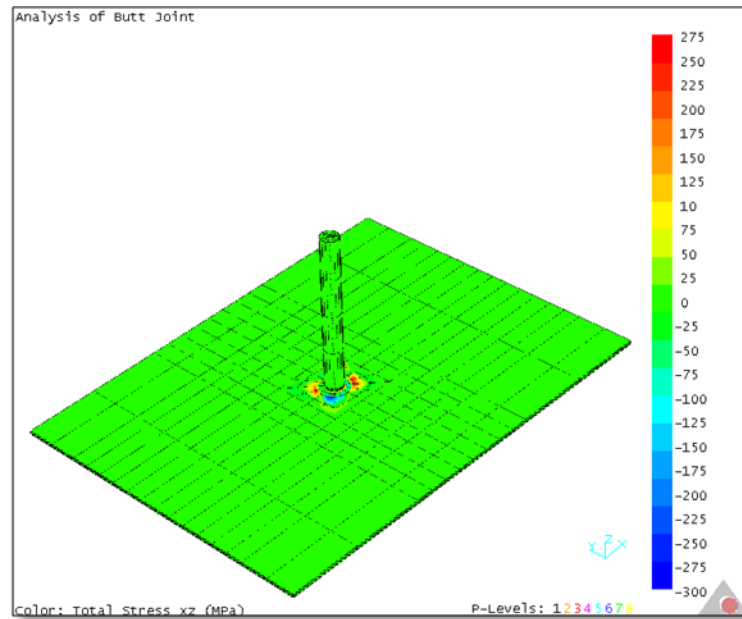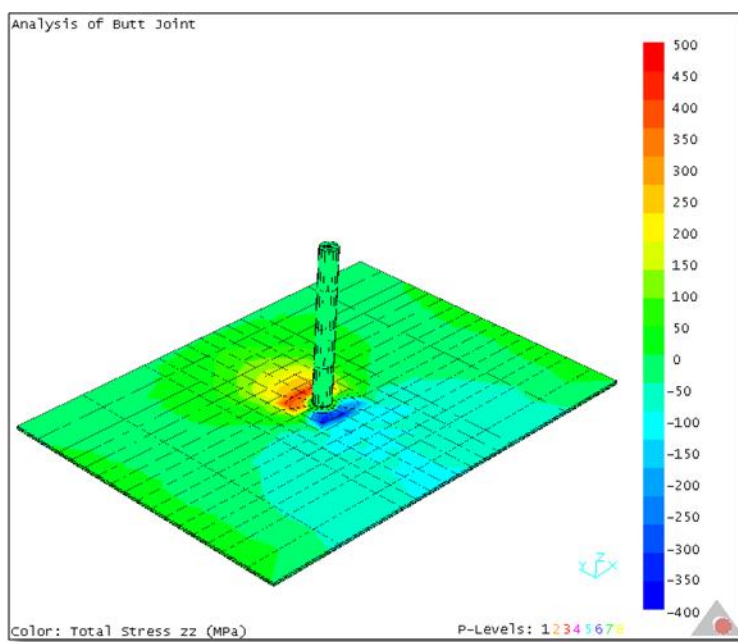

Figure 4.92 σ_z stress distribution in the AA 7075 alloy plates during welding for ω=1200 rpm and v=5 mm/s.
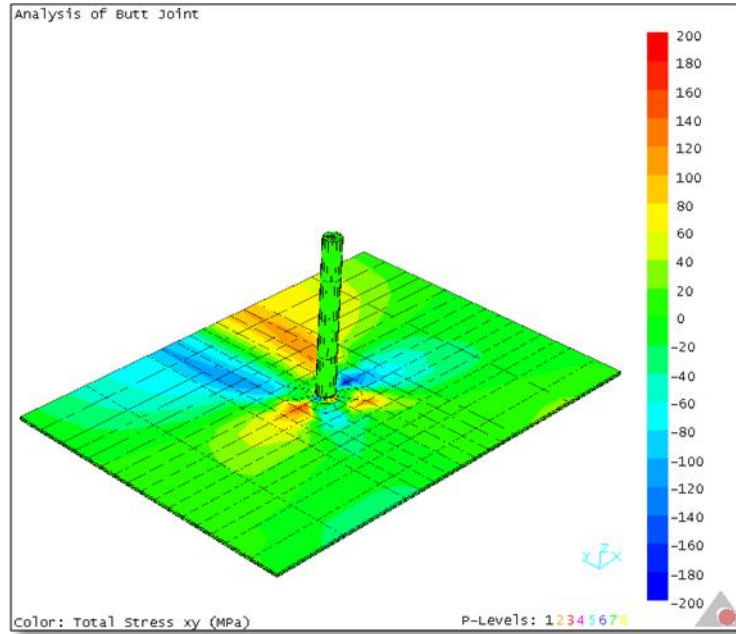
Figure 4.93 τ_{xy} stress distribution in the AA 7075 alloy plates during welding for ω=1200 rpm and v=5 mm/s.
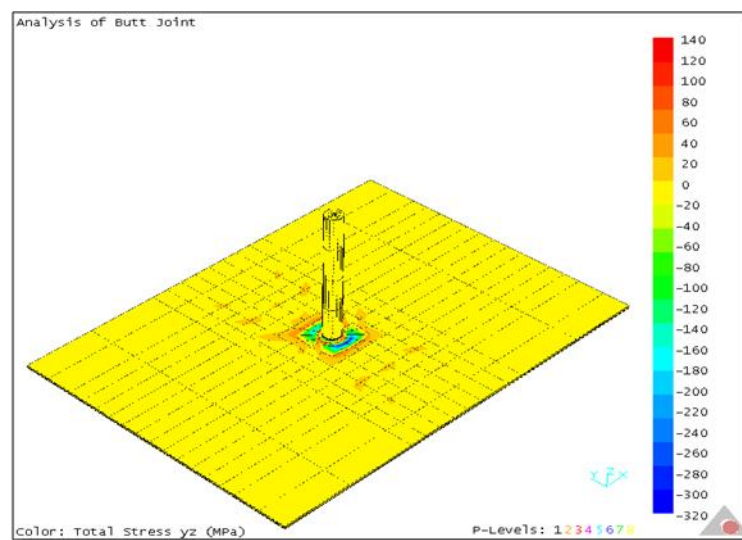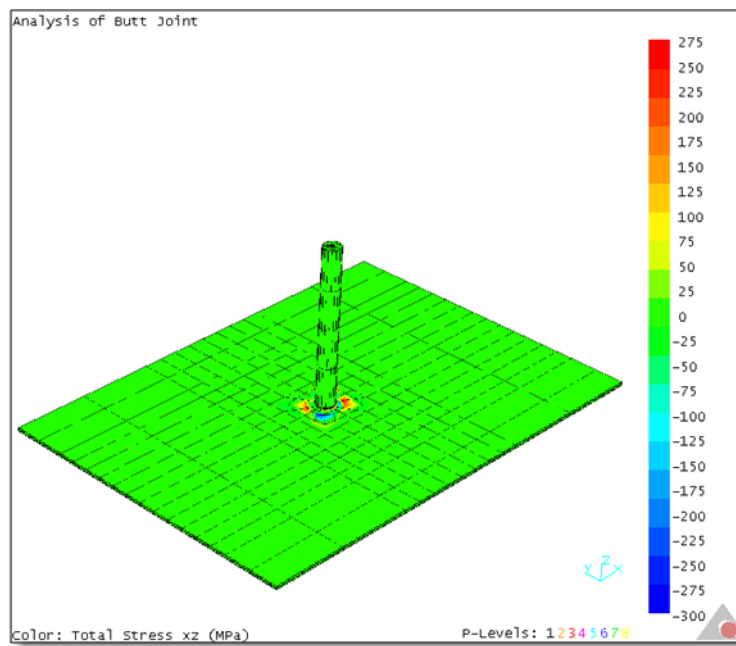

Figure 4.94 τ_{xz} stress distribution in the AA 7075 alloy plates during welding for ω=1200 rpm and v=5 mm/s.
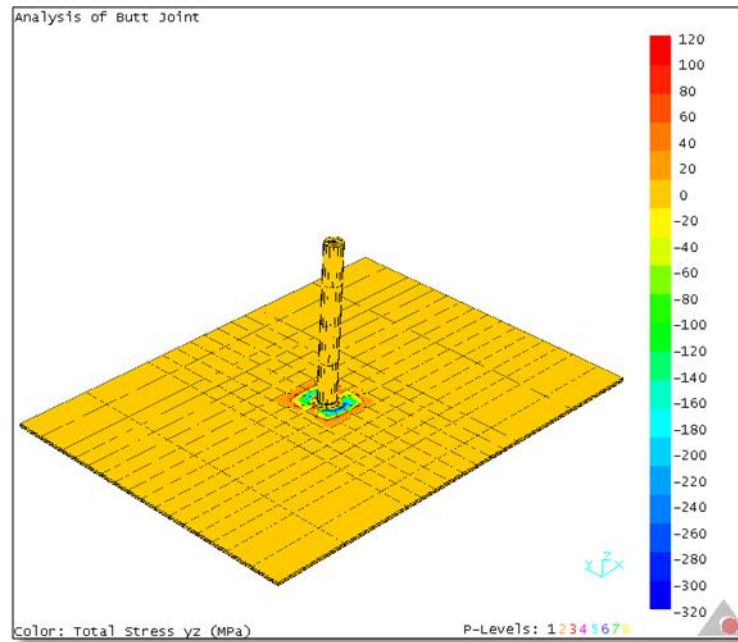
Figure 4.95 τ_{yz} stress distribution in the AA 7075 alloy plates during welding for ω=1200 rpm and v=5 mm/s.

Figure 4.96 shows the temperature variation during FSW on x, y, z coordinate plane coordinates (0;0;0), (0;10;0), (0;20;0), (0;30;0), (0;40;0) [mm].
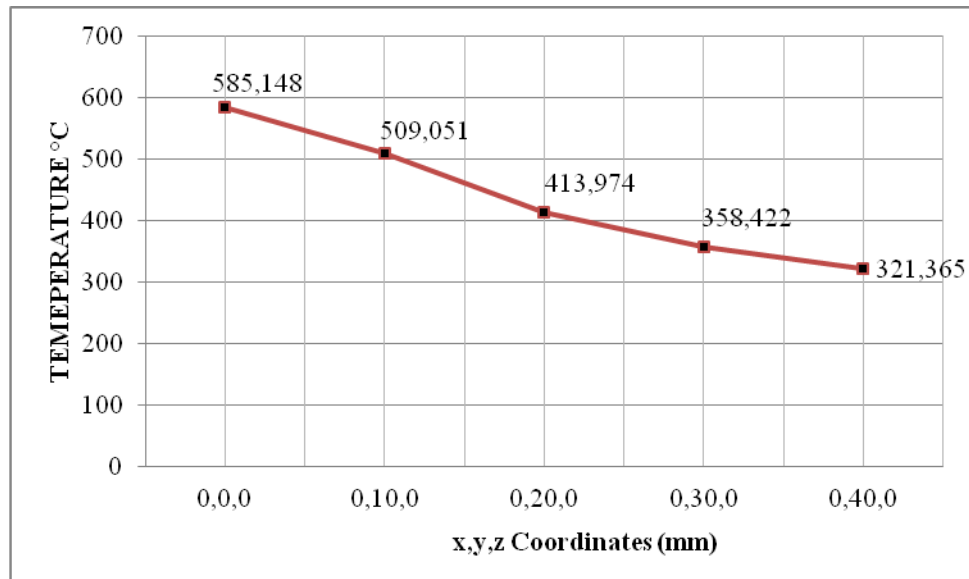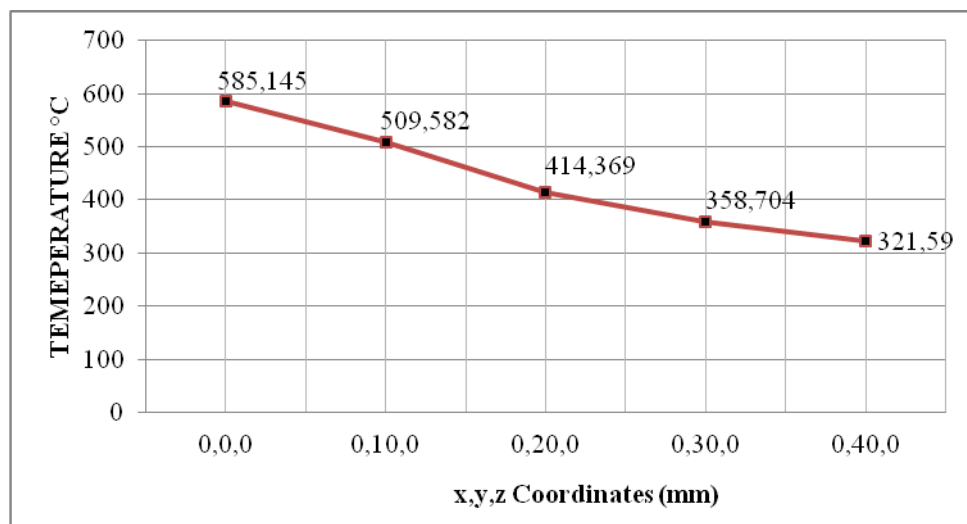

Figure 4.96 Temperatures at different coordinates for AA 7075 ω= 1200 rpm and v = 5 mm/s

Tables 13 and 14 show the maximum temperature and stress values occurred in AA 6061 and AA 7075 plates during for all welding conditions, respectively. As

seen from the tables, temperature and stress values incerase as the transverse speed decreases and rotational speed increases.

Tablo 4.13 The temperature and stress values in AA 6061 plate occurred during welding at different rotational and traverse speeds.

AA 6061	Welding Speed (mm/s)	Temperature (°C)	σ_x (MPa)	σ_y (MPa)	σ_z (MPa)	τ_{xy} (MPa)	τ_{xz} (MPa)	τ_{yz} (MPa)	Von Mises Stress (MPa)
800 RPM	2.5	440.355	365.198	375.394	363.553	112.771	173.682	82.805	386.447
800 RPM	5	430.572	377.237	385.315	373.070	112.320	176.842	80.585	388.927
1000 RPM	2.5	460.778	359.504	365.624	351.467	124.449	178.048	92.002	408.791
1000 RPM	5	452.443	371.199	375.766	361.010	123.038	181.210	90.257	410.531
1200 RPM	2.5	484.401	349.765	361.886	331.306	131.290	180.554	98.969	423.799
1200 RPM	5	478.449	359.315	370.269	337.963	128.291	183.262	101.865	426.696

As seen from Table 4.13, the maximum von Mises stress occurred at transverse speed of 1200 rpm and rotational speed of 5 mm/s in welding of AA 6061 aluminum plates. The highest temperature value is 484.401 °C and occurred at 1200 rpm and 2.5 mm/s. When σ_x, σ_y and σ_z normal stresses are considered, their maximum value occur at transverse speed of 5 mm/s and rotational speed of 800 rev/min, respectively.

Tablo 4.14 The temperature and stress values in AA 7075 plate occurred during welding at different rotational and traverse speeds.

AA 7075	Welding Speed (mm/s)	Temperature (°C)	σ_x (MPa)	σ_y (MPa)	σ_z (MPa)	τ_{xy} (MPa)	τ_{xz} (MPa)	τ_{yz} (MPa)	Von Mises Stress (MPa)
800 RPM	2.5	520.236	548.402	563.015	526.686	177.858	273.184	111.249	597.428
800 RPM	5	517.685	554.375	570.063	530.269	178.305	274.816	112.289	600.817
1000 RPM	2.5	564.086	526.044	523.498	496.966	182.858	272.077	115.328	602.551
1000 RPM	5	562.098	531.220	526.758	500.238	183.262	273.619	112.222	603.307
1200 RPM	2.5	608,795	486.072	467.412	449.486	183.003	266.104	98.969	585.912
1200 RPM	5	608,288	489.731	469.490	451.686	183.291	267.209	119.415	599.045

As seen from Table 4.14, the maximum von Mises stress occurred at transverse speed of 1000 rpm and rotational speed of 5 mm/s in welding of AA 7075 aluminum plates. The highest temperature value is 608.795 °C and occurred at 1200 rpm and 2.5 mm/s. When σ_x, σ_y and σ_z normal stresses are considered, their maximum value occur at transverse speed of 5 mm/s and rotational speed of 800 rev/min, respectively.

Comparing the results presented in Table 4.13 and 4.14, as the rotational speed increases, the temperature of the welding area increases, and as the traverse speed increases, the temperature of the welding area decreases. Bilgin and Meran have obtained similar results in their experimental studies (Bilgin and Meran, 2011).

As seen from Table 4.13 the temperature values differ between 440 °C and 478 °C in the welding of AA 6061 aluminum alloy plates. Vapakomma has found the

temperature values change between 455 °C and 470°C in his study as well (Vepakomma, 2006).

It is observed that AA 7075 aluminium alloys reach higher temperature and stress values when the results of AA 6061 and AA 7075 aluminum alloys that were analysed under the same conditions. Also, when the results obtained from the analyses are compared, the maximum temperature value generated during joining of AA 6061 aluminium alloy with FSW is much lower than the maximum temperature generated from joining of AA 7075 aluminium alloy with FSW.

CONCLUSIONS

In this study, FSW was modelled and analysed using HyperMesh and HyperXtrude softwares. Temperature and stress distributions during welding were determined by these analyses. The results obtained from this thesis are stated below:

- ➤ As the transverse velocity increases, temperature in the weld region decreases.
- ➤ As the rotational velocity increases, temperature in the weld region increases.
- ➤ As the transverse velocity increases, Von Mises stress in the weld region increases.
- ➤ As the transverse velocity increases, σ_x, σ_y and σ_z in the weld region increases.

REFERENCES

Bilgin, M.B., & Meran, C. (2011). The effect of tool rotational and traverse speed on friction stir weldability of AISI 430 ferritic stainless steels. *Materials and Design, 33,* 376–383.

Cayless, R.B.C. (1992). Alloy and temper designation systems for aluminum and aluminum alloys. *In ASM handbook (volume 2): Properties and selection: Nonferrous alloys and special-purpose material (23-101).USA: ASM International.*

Chen, C.M., & Kovacevic, R. (2003). Finite element modeling of friction stir welding—thermal and thermomechanical analysis. *International Journal of Machine Tools & Manufacture, 43,* 1319–1326.

Friction Stir Welding (n.d.) retrieved February 2, 2012 from
http://www.twi.co.uk/technologies/welding-coating-and-material processing/friction-stir-welding/

Mishra, R.S.& Ma, Z.Y. (*2005).* Friction stir welding and processing. *Materials Science and Engineering, R 50,* 1–78.

Song, M. & Kovacevic, R. (2002). Thermal modeling of friction stir welding in a moving coordinate system and its validation. *International Journal of Machine Tools & Manufacture, 43,* 605–615.

Soundararajan, V., Zekovic, S., & Kovacevic, R.(2005). Thermo-mechanical model with adaptive boundary conditions for friction stir welding of AA 6061. *International Journal of Machine Tools & Manufacture, 45,* 1577–158.

Ulysse, P. (2002). Three-dimensional modeling of the friction stir- welding process. *International Journal of Machine Tools & Manufacture, 42,* 1549–155.

Vepakomma. K. H. (2006). Three dimensional thermal modeling of frictıon stir processıng. *The florida state university college of engineering.*

Zhang, H.W., Zhang Z., & Chen, J.T. (2005). The finite element simulation of the friction stir welding process. *Materials Science and Engineering, A 403,* 340–348.

Zhu, X.K., & Chao, Y.J. (2003). Numerical simulation of transient temperature and residual stresses in friction stir welding of 304L stainless steel. *Journal of Materials Processing Technolog, 146,* 263–272.

Zhang, Z., & Zhang, H.W. (2008). Numerical studies on controlling of process parameters in friction stir welding. *Journal of materials processing technology, 209,* 241–270.